Research Paper

Geosphere, published online on 10 June 2015 as doi:10.1130/GES01156.1

GEOSPHERE

GEOSPHERE; v. 11, no. 4

DOI:10.1130/GES01156.1

6 figures; 4 tables; 1 supplemental file

CORRESPONDENCE: maellis@live.unc.edu

CITATION: Ellis, M.A., and Barnes, J.B., 2015, A global perspective on the topographic response to fault growth: Geosphere, v. 11, no. 4, doi:10.1130/GES01156.1.

Received 21 November 2014
Revision received 27 March 2015
Accepted 13 May 2015

A global perspective on the topographic response to fault growth

Magdalena A. Ellis and Jason B. Barnes*

Department of Geological Sciences, University of North Carolina, Chapel Hill, North Carolina 27599, USA

ABSTRACT

Precise factors controlling the coevolution of deformation and topography in tectonically active landscapes remain poorly understood due to complex feedbacks between numerous possible variables. Here we examine the links between fault kinematics, emergent topography, and environmental factors on a global data set of active fault-driven mountain ranges (n = 41). Using simple regressions between tectonic, climatic, and topographic variables, we explore the controls on fault-driven landscape development at the range scale. For each fault in our Google Earth accessible database, we compiled (1) topographic metrics from a 30-m digital elevation model including along-strike changes in elevation and relief, fault length, and tip zone length (the along-strike distance from fault tip to where the associated relief stops increasing) and gradient; (2) long-term (10^{4-6} yr) tectonic variables including fault slip rate, displacement rate, displacement, and age; (3) climatic variables including annual precipitation; and (4) rock type from geologic maps. Our results show that all mountain ranges reach a uniform value of relief within some distance from their tips and the length scale of this relief growth correlates with long-term vertical displacement rate (R = 0.55) and slip rate (R = 0.51). We apply a well-established framework for fault growth as the tectonic boundary condition to estimate the time required to achieve this uniform relief (~10^{4-6} yr) and suggest that this threshold time indicates regional tectonomorphic equilibrium. Strong correlations between annual precipitation and deformation rates (R > 0.60), and between lithologic strength and mountain relief (R > 0.70), allude to other principal forces affecting emergent landscape form that are often ignored. Our findings demonstrate that fault-driven topography always saturates in relief, suggest there are quantifiable fault-kinematic controls on landscape form, and hint that landscape relief patterns may, in turn, be used to estimate rates of faulting.

INTRODUCTION

Mountain belts possess diverse topographies that hold important clues about the tectonic and climate-driven erosion processes that shape them. Many studies of these landscapes have focused on the relative effects of relief or climate on erosion without explicitly considering tectonics (Ahnert, 1970; Pinet and Souriau, 1988; Montgomery and Brandon, 2002; Willenbring and von Blanckenburg, 2010). Other attempts have been made to relate worldwide mountain belt topography (orogen scale, thousands of km) to quantitative measures of both tectonics and climate (Champagnac et al., 2012). At the orogen scale, climatic and tectonic variables (mean annual precipitation, latitude, and shortening rates) can explain only limited variance (<50%), presumably because substantial complexities exist at this large scale (e.g., Champagnac et al., 2012). Perhaps as a result, most research addressing the relative roles of tectonics and climate in shaping landscapes has maintained a more regional focus, considering single mountain belts and often neglecting lithologic variations (Dahlen and Suppe, 1988; Montgomery et al., 2001; Stolar et al., 2006; Carretier et al., 2013). However, even a single region often encompasses multiple structures that overprint each other in space and time (Mouslopoulou et al., 2009; Pavlis et al., 2014). An alternative, more tractable approach to explore how topography and tectonics are linked is to focus on individual structures and their smaller (10–100 km fault trace length), emergent landforms associated with the earliest phases of fault growth (e.g., Barnes et al., 2011).

Across the globe, individual mountain ranges within a given tectonic setting tend to display similar morphologies to neighboring ranges, with equivalent widths, lengths, and relief (e.g., the U.S. Basin and Range Province; Ellis et al., 1999). These landscapes reflect feedbacks between tectonic processes that raise Earth's surface and erosive processes that lower it (Schmidt and Montgomery, 1995; Montgomery and Brandon, 2002). For example, the tectonically driven uplift of mountain ranges increases relief, leading to enhanced erosion by concentration of erosional mechanisms such as river incision and landsliding (Ahnert, 1970; Willett and Brandon, 2002). Within a tectonic province, environmental factors controlling these feedbacks (e.g., isostasy, climate, lithology, tectonic topography, and crustal properties) tend to be the same; so it is not surprising that the ensuing morphologies are also similar. However, similarities that span across tectonic settings are more intriguing. For example, research continues to address the fact that topographic relief eventually reaches a limit within small, simple ranges as well as orogenic belts, regardless of the tectonic setting (Densmore et al., 2004; Densmore et al., 2007b; Stolar et al., 2007; Burbank and Anderson, 2012; Champagnac et al., 2012). This global-scale observation indicates that there may be more universal controls determining how deformation and topography are linked.

Observations of both fault growth and topographic growth are beginning to reveal how they are linked. Step one is the recognition that faults grow in systematic ways. Faults tend to exhibit predictable relationships between their spatiotemporal variations in length, offset, and slip rate. For example, fault displacement scales linearly

*Present address: Landscape Analytics LLC, Raleigh, North Carolina 27607, USA.

Geosphere, published online on 10 June 2015 as doi:10.1130/GES01156.1

with length regardless of fault type (Cowie and Scholz, 1992a, 1992b; Dawers et al., 1993; Schlische et al., 1996; Gupta and Scholz, 2000). At the earliest stages of growth, faults grow laterally by tip propagation; when fault segments begin to interact with neighboring segments, the stress field is altered, and those in favorable spatial arrangements will experience an increase in displacement rates. The result is an integrated displacement gradient that increases from zero at the fault tips to central maxima (Fig. 1A; Dawers and Anders, 1995; Cowie, 1998; McLeod et al., 2000; Cowie and Roberts, 2001; Roberts et al., 2004). Due to mechanical breakdown and decreased friction along a fault plane, slip rate follows a similar pattern with highest slip rates in the fault center and tapering to zero at the tips (Cowie, 1998; Cowie and Shipton, 1998). A few studies have exploited this simple fault-growth framework as a tectonic boundary condition to examine the topography of isolated, emergent mountain ranges associated with active fault systems (e.g., Densmore et al., 2004; Densmore et al., 2007a; Barnes et al., 2011). They observed that (1) faulting and relief remain correlated within some distance from the tips (called the "tip zone") but become disconnected toward the along-strike center (Fig. 1B), and (2) the temporal scale over which faulting and topography remain connected within the tip zone, and by proxy the timescale to reach topographic steady state, can be estimated by substituting space for time (Harbor, 1997; Densmore et al., 2004, 2007b; Barnes et al., 2011).

In this paper we use a worldwide data set of fault-driven mountain ranges to better quantify the relative contribution of tectonics, climate, and lithology in shaping the topography of mountain ranges. Consideration of our results within the established conceptual framework for fault growth leads to new ideas on the temporal scales of mountain relief growth. We note this contribution is the first comprehensive, global analysis of patterns of along-strike relief development for active dip-slip faults. In order to best exploit the existing conceptual models for fault growth as a boundary condition (Fig. 1A), we focus on active, isolated faults or fault systems (after Barnes et al., 2011) and use long-term ($10^{4–6}$ yr) tectonic rates to understand the landforms they produce rather than less representative short-term geodetic rates (Friedrich et al., 2003). We find significant correlations between topographic metrics and independent variables (i.e., tectonic rate, climate, and lithology), which lead to new insights about the relative importance of each in shaping fault-driven landscapes.

DATA AND METHODS

Ranges

We examined 41 mountain ranges evolving in response to active dip-slip faults from diverse tectonic and climatic settings across the globe (Fig. 2). We attempted to choose a representative population of mountain ranges from regions with different tectonic settings and rates, but our strict criteria made it impossible to include every tectonic

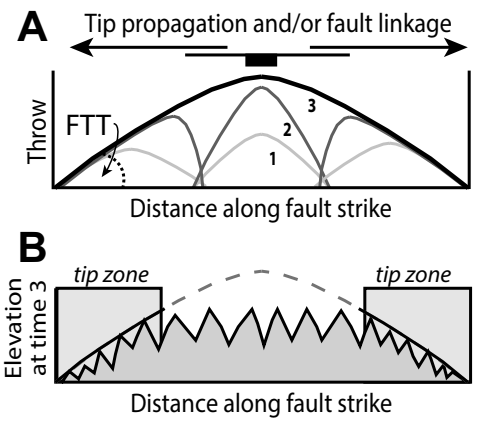

Figure 1. Schematic along-strike fault and topographic growth (time steps 1–3; simplified from Densmore et al., 2007b). (A) Along-strike profile of fault throw. Black numbers are progressive time steps 1–3, corresponding to the gray curves. FTT—Fault tip taper is the angle the displacement profile makes with horizontal. (B) Displacement (gray dashed line) and topography at time step 3, showing relief increase within the tip zones compared to uniform relief within the range center.

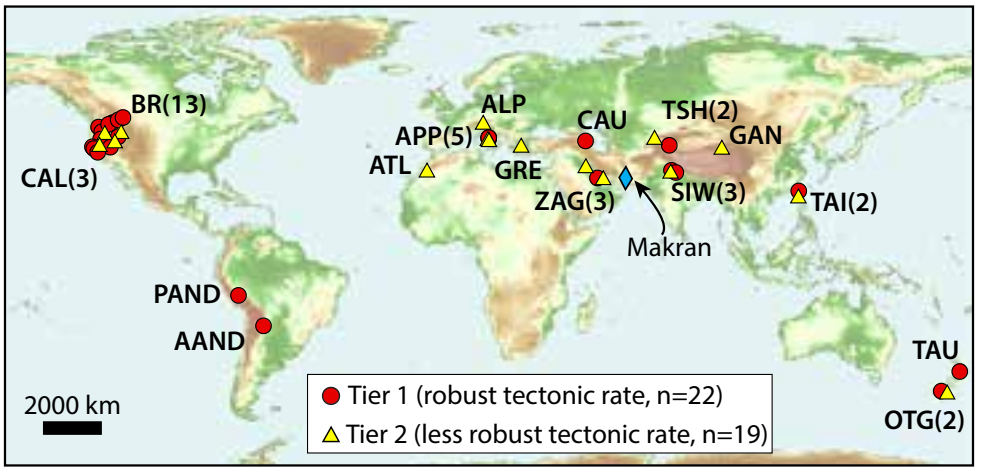

Figure 2. Fault-driven ranges studied (see text for explanation of Tiers). Names, locations, fault types, data sources, and all tectonic variables are shown in Table 1, and all topographic variables, climate variables, and lithologic ranking are shown in Table 2; all data are compiled and visible in the Supplemental File (see footnote 1). Number in parentheses—number of ranges analyzed in the region (no number means n = 1). Diamond is a fault in the Makran Region, Iran. Abbreviations: BR—Basin and Range, USA; APP—Apennines, Italy; OTG—Otago, New Zealand; ZAG—Zagros, Iran; SIW—Siwalik Hills, India; CAL—San Joaquin Basin, California; TAI—Taiwan; TSH—Tien Shan, China and Kyrgyzstan; PAND—Andes, Peru; AAND—Andes, Argentina; ATL—Atlas Mountains, Morocco; GRE—Gulf of Corinth, Greece; ALP—European Alps, Italy; GAN—Gansu Province, China; CAU—Caucasus, Azerbaijan; TAU—Taupo, New Zealand.

Geosphere, published online on 10 June 2015 as doi:10.1130/GES01156.1

region and limit the size of our data set to n = 41. We built this database using the following range selection criteria: (1) long-term (geologic, >10^4 yr) fault slip rate estimates exist; (2) the mountain range has at least one unimpeded fault tip zone; and (3) the topography is not obviously inherited, thus it can be assumed to result from the observed active faulting alone (e.g., Densmore et al., 2004). The analyzed mountains have average fault trace lengths of 81 km (16–350 km) and are on average ~5× the length of the measured tip zone. We divided the chosen ranges into two tiers based on the quality of the available fault kinematic data. Tier 1 ranges (n = 22) have reliable long-term slip rate data (i.e., thermochronology with structural mapping and reconstructions), whereas Tier 2 (n = 19) consists of ranges for which ideal long-term fault slip data are unavailable (i.e., geomorphic analysis or less than ideal geochronologic sampling locations), the kinematics are more complex (i.e., oblique slip), or the morphology could be partially inherited. For each range, we compiled data including fault geometry and kinematics, topographic variables, climatic data, and lithology (Tables 1 and 2). We also include all data and imagery in the Supplemental File[1].

Tectonics

We compiled fault type, slip rate, vertical displacement rate, vertical displacement magnitude, and fault age for each mountain range with several considerations in mind to ensure database integrity. The first consideration is that published tectonic slip rates are difficult to compile and compare due to inconsistent nomenclature (e.g., slip, throw, uplift, etc.) and differing methods by which they were estimated (e.g., thermochronology, seismic reflection data, geologic mapping, etc.). We strived to compile tectonic rate data in a way to ensure that the type of rate reported for each structure is comparable. We carefully distinguished between slip rate (fault-parallel motion) and vertical displacement rate (vertical component of slip). For brevity, we use the term "displacement" for the remainder of this paper to refer to the vertical component of slip. Our compiled values for displacement reflect maximum displacement on the structure and were either (1) reported explicitly in the original data source, (2) inferred from geologic cross sections and maps, or (3) calculated from reported deformation rate and age. Slip and deformation rate reflect the long-term average and were either (1) reported explicitly in the original data source or (2) calculated using slip or displacement and age determinations reported in the original data source. We acknowledge that using a long-term average for tectonic rate can introduce uncertainty, particularly for older faults that have long recurrence intervals, but a long-term average rate is most appropriate for comparison to range-scale topographies spread across the globe. If the original data source only reported slip rate or displacement rate, we calculated the other value using either the reported fault angle or estimated it using Anderson's theory of faulting for approximating fault angle (Anderson, 1905). Similarly, if fault displacement was not reported, we estimated it using a linear scaling relationship between fault displacement (D) and length (L) for dip-slip faults >1 km long (D = L*0.03; Schlische et al., 1996; Densmore et al., 2004). Specifics of each location are collated in the Supplemental File (see footnote 1). Although using these models to relate fault-plane parallel slip and the vertical component of slip introduces uncertainty, they are useful estimates from a brittle deformation mechanics perspective (Scholz, 2002).

The second consideration is that the underlying control on topographic growth driven by faulting is the relative vertical displacement rate in the footwall compared to the hanging wall (for a normal fault, opposite for a reverse fault) because that is what sets local base level and hence affects the landscapes erosional response to slip (e.g., Barnes et al., 2011). We acknowledge that fault geometry can significantly affect the corresponding topography. The topography we observe may not be entirely attributable to slip on the underlying fault, particularly for thrust faults where fault-bend folding may result in cessation of topographic growth (i.e., surface uplift) once slip exceeds the vertical dimension of the ramp. Unfortunately, we cannot rule out that fault-bend folding is not a factor in some of the mountain ranges we analyzed (e.g., Coalinga fold, California; see the Supplemental File [see footnote 1] for details). However, by reporting the vertical displacement on a fault (as opposed to total slip) we attempt to focus on the dimension of fault growth that primarily contributes to topographic development. We include the fault geometry of every analyzed structure in the Supplemental File (see footnote 1) for reference. We also assume that our compiled tectonic rates are the best estimates of relative displacement rate because (1) studies rarely measure tectonic rates explicitly in both the hanging walls and footwalls as well as footwall sedimentation rates; (2) it is beyond the scope of this paper to independently measure such rates; and (3) our principal intent is to explore the links between tectonic and topographic metrics that are the most commonly available.

Topography

We used the advanced spaceborne thermal emission and reflection radiometer (ASTER) 30-m global digital elevation model (DEM) (METI and NASA, 2012) to conduct the topographic analysis. Variables we measured include tip zone length and gradient, maximum and uniform relief, fault trace length, and along-strike changes in elevation and relief (Fig. 3; Supplemental File [see footnote 1]). We manually clipped the DEM based on the topographic extent of each mountain range (Fig. 3A) and then collected one-pixel (~30-m)–wide swaths perpendicular to the strike of the fault. We extracted along-strike minimum, mean, and maximum elevation and relief (defined as max–min elevation) profiles (Figs. 3B and 3C; see the Supplemental File [see footnote 1] for all profiles) and finally measured remaining parameters from these profiles (tip zone length and gradient). For example, tip zone length is the along-strike distance from the fault tip to the point where the relief stops increasing (Fig. 3C); this key metric is the scale over which topography reaches a steady form (Densmore et al., 2004; Densmore et al., 2007b). We developed a quantitative method for selecting the along-strike location where relief transitions from increasing

[1]Supplemental File. Google Earth (.kmz) file that includes every mountain range in the presented database along with all their tectonomorphic and climatic values. Please visit http://dx.doi.org/10.1130/GES01156.S1 or the full-text article on www.gsapubs.org to view the Supplemental File.

Geosphere, published online on 10 June 2015 as doi:10.1130/GES01156.1

TABLE 1. TECTONIC VARIABLES FOR EACH RANGE AND CORRESPONDING REFERENCES

Range	Tier	Fault type	Slip rate (km/m.y.)	Vertical displacement rate (km/m.y.)	Tip zone (km)	Vertical displacement (km)	Age of onset (Ma)	Method used	Reference
Aguaragüe Range, Argentina	1	T	2	1*	22	2.5–3	2.5–3	S,m,s,w,o	Echavarria et al. (2003) and references therein
Beaverhead Range, Idaho	1	N	0.3	0.25*	10	5–6	5.4	S,i	Densmore et al. (2004, 2007b); Anders et al. (1993)
Chandigarh fold, India	1	T	6.3	4–6	5	2.7–3.8	0.63	S,r,p,m,w	Barnes et al. (2011); Malik and Nakata (2003)
Coalinga fold, California	1	T	0.5–3	1.1	9.5	2.5	2.2	S,s,w	Guzofski et al. (2007); Namson and Davis (1988)
Jackson Mountains, Nevada	1	N	0.6	0.4	14.7	4.5–5.4	12	S,T	Colgan et al. (2006)
Kashi anticline, China	1	T	3.6*	1.8	13	2.5	1.4	S,m	Chen et al. (2007); Scharer et al. (2006)
Kettleman Hills, California	1	T	1–1.2	0.3–0.5	7	0.7–1.2§	3	S,s,w	Guzofski et al. (2007); Namson and Davis (1988)
Lemhi Range, Idaho	1	N	0.6	0.5	16	5–6	<6.5	S,T,i	Densmore et al. (2004, 2007b); Anders et al. (1993)
Liri fault, Italy	1	N	1.3*	1.1	8	2	2.5–3.3	S,p,i	Roberts and Michetti (2004)
Lost River Range, Idaho	1	N	0.3	0.25*	15	5–6	<6.5	S,i	Densmore et al. (2004, 2007b); Stein et al. (1988); Janecke et al. (1991)
Mand anticline, Iran	1	T	0.8*	0.42	7.3	2.1	5	S,w,r,s	Oveisi et al. (2007)
Mohand fold, India	1	T	13.8	6.9	6	2.3–3.2	0.78	S,r,p,m	Barnes et al. (2011); Powers et al. (1998); Wesnousky et al. (1999)
Ostler fault, New Zealand	1	T	1.2–1.9	0.3–1.2	4	0.8	2.4	S,O,C,G,s	Amos et al. (2010); Ghisetti et al. (2007); Amos et al. (2007)
Paeroa fault, New Zealand	1	N	1.7*	1.5	9.5	0.56–0.9	1–0.9	S,T,i	Nicol et al. (2006); Villamor and Berryman (2001); Berryman et al. (2008); Wilson et al. (1995)
Pakuashan anticline, Taiwan	1	T	13*	8.3	3.2	0.5	0.06	S,O	Simoes et al. (2007)
Pine Forest, Nevada	1	N	0.6	0.5*	9.5	5.3–6.9	13	S,T	Colgan et al. (2006)
Ruby Valley, Nevada	1	N	0.28*	0.24	12	2.4	<10	S,T	Colgan et al. (2010)
Santa Rosa, Nevada	1	N	0.6–0.7	0.4–0.5	10.5	5–6	12	S,T	Colgan et al. (2006)
Timpia fold, Peru	1	T	0.52	0.43	17	1.5–3	<6	S,T,s,w	Espurt et al. (2011)
Toiyabe Range, Nevada	1	N	0.2–1.0	0.3	18	4–5.5	15	S,T,G	Stockli (1999); Redsteer and Lidke (1998)
Wassuk Range, Nevada	1	N	0.7*	0.6	16	8.5	15	S,T	Stockli et al. (2002); Gorynski et al. (2013)
Wheeler Range, California	1	T	4.3	3.2	5.8	0.44	0.4	S,G,r,w	Keller et al. (1998); Medwedeff (1992)
Apennines (zone), Italy	2	N	5.1*	4.4	24	6.6	2.5–3.3	S,p,i	Roberts and Michetti (2004)
Balachaur fold, India	2	T	6	5	4.5	1.3§	~0.5	S,e,s,w	Powers et al. (1998)
Diamond fault, Nevada	2	N	<0.2	<0.15	13.6	2.1§	10–15	S,G	Redsteer and Machette (2000)
Fucino fault, Italy	2	N	2.3*	2	4.3	2.2	2.5–3.3	S,p,i	Cowie and Roberts (2001); Roberts and Michetti (2004)
High Atlas Range, Morocco	2	T	0.15	0.075	18.2	2.2§	N.D.	S,T	Balestrieri et al. (2009)
Kyrgyz Range, Kyrgyzstan	2	T	1	0.5*	44	6	11	S,T	Sobel et al. (2006); Bullen et al. (2003)
Maolin Range, Taiwan	2	T	10*	5	8.9	6	3.4	S,T	Willet et al. (2003); Fuller et al. (2006)
Mingacevir Range, Azerbaijan	2	T	2.4	1.2	6.2	2–4	3.4–1.6	S,T,i	Forte et al. (2010); Avdeev and Niemi (2011); Mosar et al. (2010)
Pilot Creek Range, Nevada	2	N	<0.2	<0.15	10	2.7§	10–15	S,G	Oswald et al. (1998)
Raggedy-Blackstone, New Zealand	2	T	0.8*	0.4	7.7	0.5–1	1.2	S,C,e	Bennett et al. (2006); Markley and Norris (1999)
S. Aksai Range, China	2	T/SS	6*	3	17	1.4§	1–5	S,G,e	Gold et al. (2006); Cowgill et al. (2004)
S. Alkyonides, Greece	2	N	2.9–3.5*	2.5–3	13	2.5–3	1	S	Morewood and Roberts (1999); Armijo et al. (1996)
Scurcola fault, Italy	2	N	0.96*	0.83	3	1.46	2.5–3.3	S,p,i	Roberts and Michetti (2004)
Trassaco fault, Italy	2	N	0.96*	0.83	5.7	1.42	2.5–3.3	S,p,i	Roberts and Michetti (2004)
Valdobbiadene, Alps, Italy	2	T	1.9	0.75	7	1.2§	N.D.	S,r,e	Benedetti et al. (2000)
W. Humboldt Range, Nevada	2	N	<0.2	<0.15	13	1.7§	10–15	S,G	Adams and Sawyer (1999)
White Mountains, California	2	N/SS	0.9	0.7	20	8	12	S,T	Stockli et al. (2003)
Zagros KSD fold, Iran	2	T	<1	0.25	17	1–2	8	S,G,g,m	Blanc et al. (2003); Ramsey et al. (2008); Allen et al. (2004); Homke et al. (2004)
Zarrinabad fold, Iran	2	T	0.7–0.8	0.4	7.3	3	8.1–7.2	S,G,g,m	

Note: Fault type: N—normal fault; T—thrust fault; SS—strike-slip fault. Method used: T—thermochronology; S—structural mapping; p—paleoseismologic trenching; O—optically stimulated luminescence (OSL); r—radiocarbon; m—magnetostratigraphy; G—geomorphic analysis; w—well; s—seismic; C—cosmogenic nuclides; g—geodetics; i—isotopic dating; o—oxygen isotopes; e—extrapolated from proximal structures. N.D.—No data.

*Either slip or uplift rate was reported in literature; the starred rate was then calculated using fault angle.

§Vertical displacement is estimated using a linear scaling relationship between fault displacement and length: $D = L \times 0.03$ (Schlische et al., 1996).

Geosphere, published online on 10 June 2015 as doi:10.1130/GES01156.1

TABLE 2. TOPOGRAPHIC, CLIMATIC, AND LITHOLOGIC VARIABLES FOR EACH RANGE

Range	Tip zone length (km)	Maximum relief, R_{MAX} (m)	Uniform relief, R_U (m)	Maximum elevation, E_{MAX} (m)	Minimum elevation, E_{MIN} (m)	Trace length (km)	Annual precipitation (mm/yr)	Mean monthly precipitation (mm)	Lithologic ranking	Tip zone gradient
Aguaragüe Range, Argentina	22	1310	701	1883	662	282.6	992	83 ± 74	2	0.117
Beaverhead Range, Idaho	10	1292	916	3458	1980	127.0	234	19 ± 11	3	0.092
Chandigarh fold, India	5	300	199	615	316	46.9	1256	102 ± 121	1	0.040
Coalinga fold, California	9.5	1072	898	1600	402	65.9	229	19 ± 17	1	0.095
Jackson Mountains, Nevada	14.7	1316	790	2691	1387	51.8	196	16 ± 7	5	0.079
Kashi anticline, China	13	954	860	2421	1410	61.6	112	10 ± 6	1	0.066
Kettleman Hills, California	7	276	192	406	121	38.5	170	14 ± 13	1	0.027
Lemhi Range, Idaho	16	1716	1273	3689	1788	156.9	230	19 ± 9	3	0.080
Liri fault, Italy	8	1474	1120	2041	671	55.0	933	78 ± 32	3	0.140
Lost River Range, Idaho	15	1861	1157	3820	1906	137.0	238	20 ± 8	3	0.077
Mand anticline, Iran	7.3	744	488	806	59	74.1	247	20 ± 26	2	0.067
Mohand fold, India	6	581	432	931	364	77.1	1442	119 ± 159	1	0.072
Ostler fault, New Zealand	4	390	209	880	485	34.4	994	64 ± 8	1	0.026
Paeroa fault, New Zealand	9.5	553	413	960	382	23.2	1269	118 ± 14	2.5	0.034
Pakuashan anticline, Taiwan	3.2	368	262	447	72	32.8	2103	180 ± 150	1	0.087
Pine Forest, Nevada	9.5	1110	792	2447	1331	53.9	218	17 ± 7	5	0.083
Ruby Valley, Nevada	12	1439	1068	3465	1963	99.0	401	32 ± 11	5	0.082
Santa Rosa, Nevada	10.5	1558	1071	2942	1517	88.7	275	22 ± 8	5	0.102
Timpia fold, Peru	17	3435	1145	4155	772	90.4	1690	141 ± 86	2	0.067
Toiyabe Range, Nevada	18	1746	1051	3552	1845	182.6	193	16 ± 3	5	0.081
Wassuk Range, Nevada	16	2117	1166	3407	1557	108.0	158	13 ± 4	5	0.073
Wheeler Range, California	5.8	472	390	591	241	18.1	210	18 ± 15	1	0.057
Apennines (zone), Italy	24	2735	1906	2866	161	176.8	858	71 ± 22	3	0.080
Balachaur fold, India	4.5	172	130	540	349	43.5	1026	81 ± 93	1	0.029
Diamond fault, Nevada	13.6	1178	859	3235	1890	69.7	285	23 ± 8	3	0.063
Fucino fault, Italy	4.3	771	500	1592	893	15.7	870	72 ± 16	3	0.116
High Atlas Range, Morocco	18.2	3138	2583	3605	644	72.2	225	21 ± 20	4	0.142
Kyrgyz Range, Kyrgyzstan	44	3567	2645	4859	1187	358.6	606	50 ± 19	5	0.060
Maolin Range, Taiwan	8.9	2198	1281	2644	305	34.3	1689	139 ± 133	4	0.144
Mingacevir Range, Azerbaijan	6.2	346	265	438	86	32.0	387	32 ± 11	1	0.029
Pilot Creek Range, Nevada	10	1079	651	2923	1735	89.4	195	16 ± 4	5	0.065
Raggedy-Blackstone, New Zealand	7.7	578	304	986	373	41.5	432	37 ± 9	3	0.030
S. Aksai Range, China	17	1943	1488	4993	3065	46.2	21	2 ± 2	3	0.088
S. Alkyonides, Greece	13	1366	816	1366	0	58.2	499	41 ± 27	1	0.032
Scurcola fault, Italy	3	501	271	1444	848	41.3	886	72 ± 21	3	0.090
Trassaco fault, Italy	5.7	892	585	1970	988	24.1	933	78 ± 32	3	0.084
Valdobbiadene, Alps, Italy	7	1579	1076	1754	269	40.0	1235	104 ± 28	3	0.154
W. Humboldt Range, Nevada	13	1410	984	2975	1494	55.4	181	16 ± 5	5	0.076
White Mountains, California	20	2841	1807	4330	1383	190.8	247	20 ± 6	5	0.082
Zagros KSD fold, Iran	17	1333	1001	3190	1629	80.0	359	27 ± 33	2	0.059
Zarrinabad fold, Iran	7.3	1261	842	1630	356	54.2	433	36 ± 38	2	0.112

Note: KSD—Kuh-e Sefidar.

Geosphere, published online on 10 June 2015 as doi:10.1130/GES01156.1

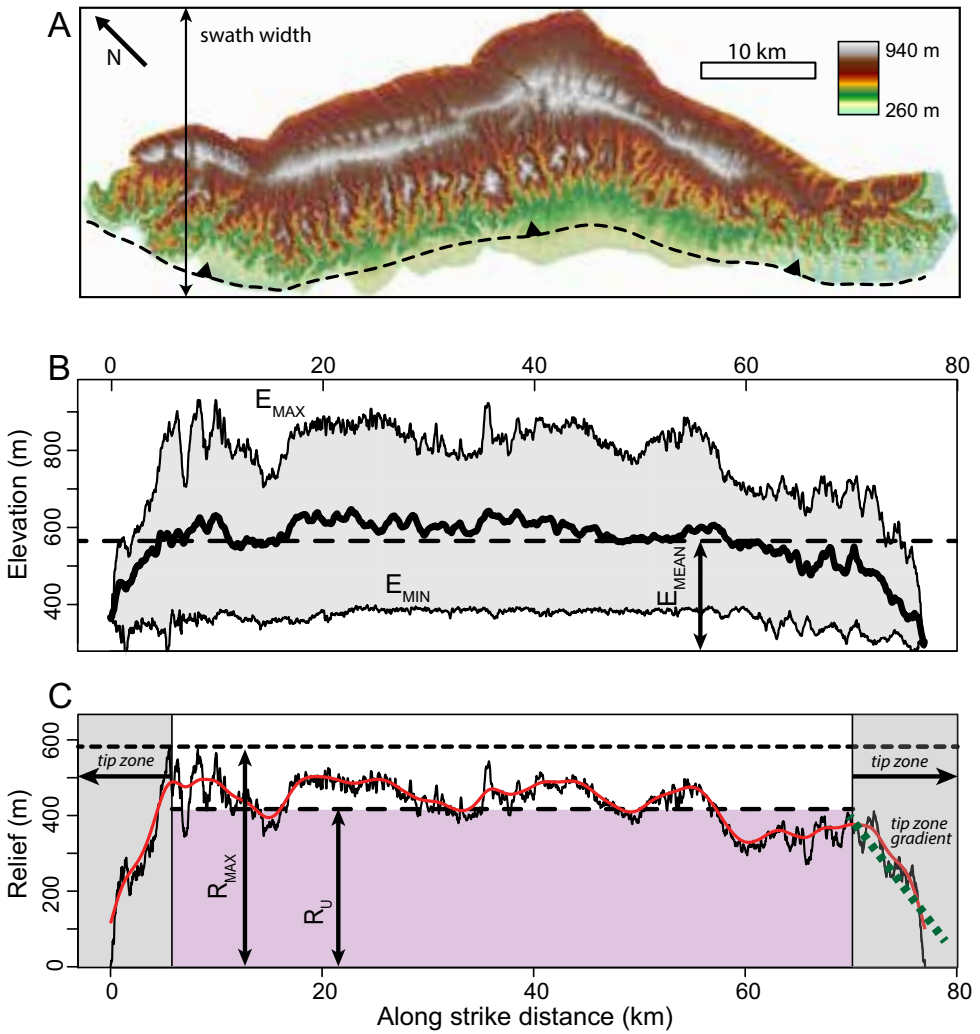

Figure 3. Range topography measurements with example application to the Mohand Range in northwest India (location SIW in Fig. 2; method after Champagnac et al., 2012; Densmore et al., 2004). (A) Isolated Mohand Range topography. (B) Swath elevation profiles along strike including maximum, minimum, and mean elevation (E_{MAX}, E_{MIN}, and E_{MEAN}). (C) Relief parameters measured are maximum relief (R_{MAX}), tip zone length, uniform relief (R_U) between tip zones (purple box), and tip zone gradient, which indicates the rate of relief growth (green dashed line). We quantitatively determined tip zone length (and hence other dependent metrics as well) by spline-smoothing (red line) the relief profile (black line) and then calculating its first major inflection from the tip.

in value to becoming uniform in order to measure and compare tip zone lengths. After smoothing the relief profile with a spline function (red line, Fig. 3C), we define the tip zone length as the first zero crossing of the first derivative. Tip zone gradient is the rate of surface elevation change within this zone (green dashed line, Fig. 3C; after Densmore et al., 2004). Uniform relief (R_U) is the mean local relief value within the fault interior (purple region in Fig. 3C) that excludes the tip zones. Fault trace length is defined as the farthest along-strike extent of range topography. Subsurface fault length may be longer than the surface fault trace particularly in thrust systems (e.g., Wells and Coppersmith, 1994; Davis et al., 2005); thus we consider fault trace length to be a topographic rather than a tectonic variable.

Climate and Lithology

To account for variations in climate, we used mean annual and monthly precipitation. Precipitation values were compiled from the Global Precipitation Climatology Centre worldwide database (GPCC Normals Version 2010; http://gpcc.dwd.de) with a 0.25° grid size (Becker et al., 2013; Schneider et al., 2014). We avoided heavily glaciated ranges. We also used a semiquantitative scale for lithologic variations across each range (1–5, weak to strong) based on the dominant exposed lithology. The ranking is based on physical and mechanical properties (uniaxial compressive/tensile strength, elastic modulus, point load index, and Schmidt hammer rebound values) generalized for rock type (Obert and Duvall, 1967; Zhang, 2005).

Data Analysis

We performed two bivariate statistical analyses on our database. First, we performed a test of linear dependence, or Pearson correlation, between all noncategorical variables (Tables 3 and 4; Davis, 2002). Second, because the lithologic strength variable is categorical, we conducted a test of monotonic dependence, or Spearman correlation,

Geosphere, published online on 10 June 2015 as doi:10.1130/GES01156.1

TABLE 3. PEARSON CORRELATION MATRIX FOR TIER 1 RANGES

	Displacement rate*	Tip zone	Vertical displacement	Age	Maximum relief	Uniform relief	Maximum elevation	Trace length	Mean monthly precipitation	Tip zone gradient	Lithology strength ranking*
Slip rate	0.98	**–0.51**	–0.37	**–0.53**	**–0.48**	**–0.53**	–0.55	–0.26	**0.64**	0.05	**–0.76**
P-value	*0.000*	***0.015***	*0.091*	***0.010***	***0.024***	***0.010***	*0.008*	*0.239*	***0.001***	*0.812*	***0.000***
Displacement rate		**–0.55**	–0.38	**–0.55**	**–0.49**	**–0.56**	–0.58	–0.32	**0.67**	0.11	**–0.64**
P-value		***0.008***	*0.082*	***0.008***	***0.019***	***0.007***	*0.005*	*0.153*	***0.001***	*0.642*	***0.001***
Tip zone			0.53	0.52	0.74	0.70	0.75	0.80	–0.29	–0.19	0.61
P-value			*0.035*	*0.064*	*0.000*	*0.001*	*0.000*	*0.000*	*0.193*	*0.419*	*0.003*
Vertical displacement				0.77	**0.52**	**0.64**	0.69	0.45	–0.49	–0.13	**0.64**
P-value				*0.000*	***0.014***	***0.001***	*0.000*	*0.036*	*0.020*	*0.556*	***0.001***
Age					**0.56**	**0.61**	0.69	0.31	**–0.51**	–0.10	**0.89**
P-value					***0.007***	***0.002***	*0.000*	*0.162*	***0.016***	*0.671*	***0.000***
Maximum relief						0.85	0.88	0.46	–0.08	0.12	**0.73**
P-value						*0.000*	*0.000*	*0.031*	*0.709*	*0.609*	***0.000***
Uniform relief							0.92	0.49	–0.39	0.28	**0.66**
P-value							*0.000*	*0.020*	*0.070*	*0.206*	***0.001***
Maximum elevation								0.52	–0.35	0.06	**0.71**
P-value								*0.012*	*0.115*	*0.776*	***0.000***
Trace length									–0.15	–0.23	0.49
P-value									*0.492*	*0.300*	*0.020*
Mean monthly precipitation										0.18	–0.27
P-value										*0.415*	*0.216*
Tip zone gradient											0.20
P-value											*0.381*

Note: Bold values are those discussed in text.
*Spearman nonparametric correlation values for lithologic robustness.

between lithologic strength and all other variables (last column, Tables 3 and 4). A Spearman correlation is a nonparametric measure of dependence and is well suited for ranked data (Spearman, 1904). For both tests, we report R and p-values. The closer the correlation coefficient, R, is to 1, the better the correlation. P-values are the probability that the results could be obtained by random chance such that lower p-values indicate a more robust correlation (Davis, 2002). We performed these analyses on Tier 1 (Table 3) and on all data (Table 4) to explore relationships between the various tectonic and topographic variables. In the discussion below, we focus on (1) the best correlations (R > 0.5; p-values < 0.01) and (2) the surprising noncorrelations, both of which lead to new insights into the links between faulting and the resultant landscape form.

RESULTS

To understand the controls of fault-driven landscapes, we investigate the statistical relationships between topographic metrics (listed above) and tectonic, climatic, and lithologic parameters using correlation statistics. Because our primary interest is to understand the controlling variables in shaping the landscape, we only elaborate on strong relationships that relate to the landscape. For brevity, we only show plots for statistically significant regressions or for those that seem to have the most meaningful insights. Below we report the R and p-values for Tier 1 data (Table 3), with the corresponding R and p-values for all data (Tier 1 + Tier 2; Table 4) in brackets immediately following.

Tip Zone Length and Faulting Rate

There is a significant (p-value < 0.01) negative correlation between tip zone length and faulting rate (Fig. 4; Tables 3 and 4). Our database includes fault slip rates from 0.15 to 13.8 km/m.y., displacement rates from 0.075 to 8.3 km/m.y., and tip zones from 3.2 to 44 km (3.2–22 km for Tier 1) long (Tables 1 and 2). In the range interiors, relief reaches mean values (R_U; e.g., Fig. 3) of ~150–2650 m. Regression between tip zone length and displacement rate shows that faster rock uplift results in shorter tip zone length (R = –0.55 [–0.36], p-value 0.008 [0.019]; Fig. 4A; Tables 3 and 4). This correlation is lower for slip rates (R = –0.51 [–0.31], p-value 0.015 [0.043]; Fig. 4B; Tables 3 and 4), presumably because it is the vertical component

Geosphere, published online on 10 June 2015 as doi:10.1130/GES01156.1

TABLE 4. PEARSON CORRELATION MATRIX FOR ALL RANGES

	Displacement rate	Tip zone	Vertical displacement	Age	Maximum relief	Uniform relief	Maximum elevation	Trace length	Mean monthly precipitation	Tip zone gradient	Lithology strength ranking*
Slip rate	0.97	**–0.31**	–0.13	**–0.48**	**–0.23**	**–0.21**	–0.36	–0.20	**0.62**	–0.02	**–0.59**
P-value	*0.000*	***0.043***	*0.408*	***0.002***	***0.146***	***0.184***	*0.023*	*0.214*	***0.000***	*0.887*	***0.000***
Displacement rate		**–0.36**	–0.13	**–0.51**	**–0.26**	**–0.24**	–0.41	–0.21	**0.64**	–0.02	**–0.52**
P-value		***0.019***	*0.414*	***0.001***	***0.103***	***0.130***	*0.008*	*0.190*	***0.000***	*0.887*	***0.000***
Tip zone			0.41	0.44	0.72	0.73	0.71	0.80	–0.29	–0.18	0.49
P-value			*0.006*	*0.003*	*0.000*	*0.000*	*0.000*	*0.000*	*0.068*	*0.237*	*0.001*
Vertical displacement				0.38	**0.56**	**0.52**	0.55	0.56	–0.25	–0.17	0.46
P-value				*0.016*	***0.000***	***0.000***	*0.000*	*0.000*	*0.117*	*0.276*	*0.003*
Age					**0.53**	**0.58**	0.59	0.27	**–0.47**	–0.04	**0.79**
P-value					***0.000***	***0.000***	*0.000*	*0.092*	***0.002***	*0.806*	***0.000***
Maximum relief						0.93	0.83	0.60	–0.09	0.08	**0.64**
P-value						*0.000*	*0.000*	*0.000*	*0.596*	*0.613*	***0.000***
Uniform relief							0.80	0.60	–0.23	0.11	**0.60**
P-value							*0.000*	*0.000*	*0.146*	*0.481*	***0.000***
Maximum elevation								0.56	–0.36	0.06	**0.70**
P-value								*0.000*	*0.022*	*0.712*	***0.000***
Trace length									–0.14	–0.28	0.39
P-value									*0.367*	*0.081*	*0.011*
Mean monthly precipitation										0.25	–0.34
P-value										*0.113*	*0.031*
Tip zone gradient											0.29
P-value											*0.065*

Note: Bold values are those discussed in text.
*Spearman nonparametric correlation values for lithologic robustness.

of rock motion that affects relief growth the most. However, no topographic metric shows any significant trend related to fault type. At low faulting rates (<~1 km/m.y.), the increased scatter in tip zone length may be related to regional-to-local factors such as lithology and climate. For example, the White Mountains, California, have one of the largest tip zones (20 km) and are (1) classified as arid, cold desert (Kottek et al., 2006) and (2) made up of hard granitic and metamorphic rock (Tables 1 and 2) (Stockli et al., 2003). Overall, the main results are that the faster the fault slips, the shorter the distance over which relief saturates (tip zone distance) and that regional-scale factors such as climate and lithology may impart influence on some of the more extreme outlier tip zones in a predictable way.

Precipitation and Deformation Rate

Two of the strongest correlations in our database are between precipitation and slip rate and precipitation and displacement rate (R = 0.64 [0.62] and 0.67 [0.64]; p-value = 0.001 [0.000] for both; Fig. 4C; Tables 3 and 4). Documented mean monthly precipitation ranges from 2 ± 2 mm/month (21 mm/yr mean annual; S. Aksai Range, China) to 180 ± 150 mm/month (2103 mm/yr mean annual; Pakuashan anticline, Taiwan). Here we define the uncertainty as one standard deviation, which reflects the seasonal variability in rainfall. For example, the S. Aksai Range, China, receives <1 mm/month of precipitation for ~8 months out of the year. The positive correlation indicates that mountain ranges with faster faulting rates tend to also have higher rates of precipitation. Precipitation also has a moderately significant negative correlation with age of faulting (R = –0.51 [–0.47], p-value = 0.016 [0.002]), with younger locations tending toward higher amounts of precipitation (Table 2). Collectively, these results statistically link rainfall, tectonic rates, and age of faulting.

Tip Zone Gradient

Tip zone gradient (relief increase per unit tip zone length, Fig. 3C) has no correlation with any other non-landscape variable in our database (Tables 3 and 4). The strongest correlation is between tip zone gradient and lithology, but it is a poor correlation at best (R = 0.29 [0.24], p-value =

Geosphere, published online on 10 June 2015 as doi:10.1130/GES01156.1

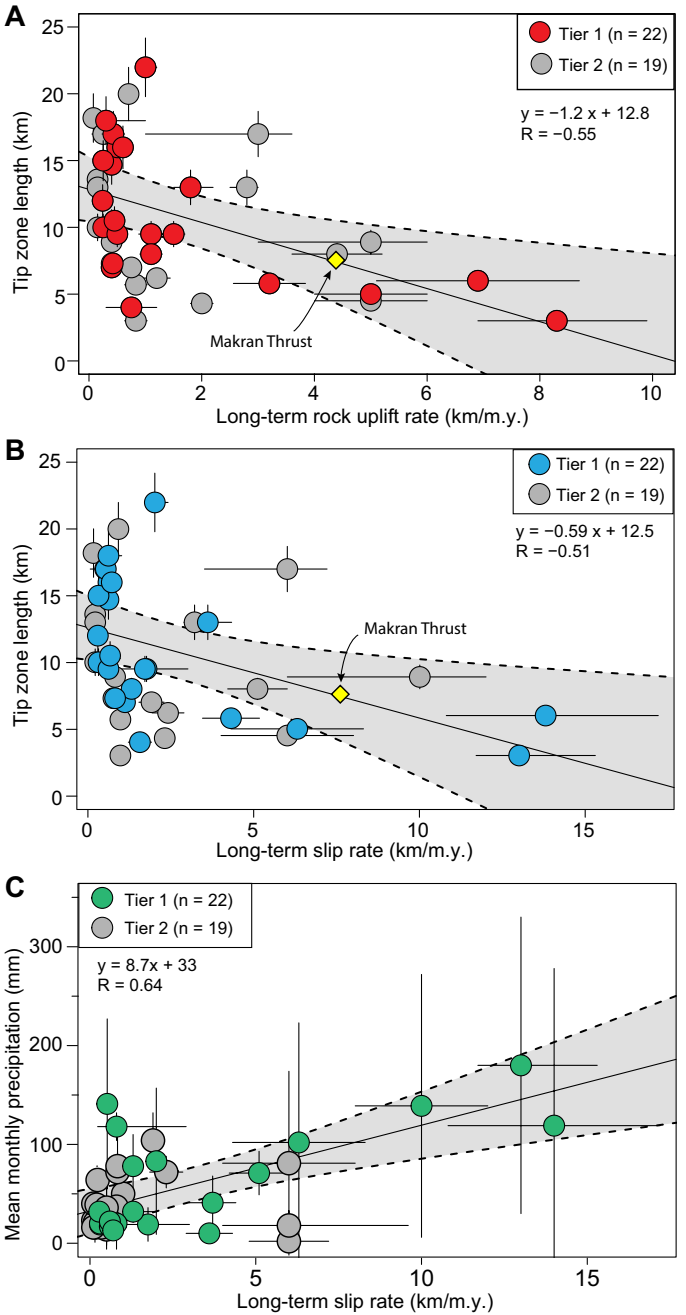

Figure 4. Plots for high correlations (R > 0.5; p-value ≤ 0.01) between tectonic, topographic, and climatic variables. Rock uplift and slip rate error bars are uncertainties as reported in the literature (see Table 1). Regression lines are fit to Tier 1 data only with uncertainty envelopes (gray zones) at 95% confidence. Tip zone length versus (A) rock uplift rate and (B) long-term slip rate. (C) Mean monthly precipitation versus long-term slip rate. Error bars on precipitation are 1σ and show the seasonal variation in precipitation.

0.210 [0.122], Tables 3 and 4). Tip zone gradient has a mean value of 0.076 and a standard deviation of 0.033 (Table 2; Fig. 5A). The maximum value is 0.15, and the minimum is 0.026. There is little variation in tip zone gradient—the majority (80%) of values fall between 0.05 and 0.15—suggesting that this parameter converges around a common value.

Relief and Tectonic Variables

There are moderate-to-strong correlations (R = ~0.5–0.6) between measures of relief (R_U and R_{MAX}) and tectonic variables (slip and displacement rate, total displacement) (Tables 3 and 4). Both R_U and R_{MAX} have negative correlations with slip rate (R = –0.53 [–0.21], R = –0.48 [–0.23], respectively) and displacement rate (R = –0.56 [–0.24], R = –0.49 [–0.26], respectively). Relief metrics have slightly stronger correlations with magnitude of displacement (R = 0.52 [0.56] for R_{MAX}; R = 0.64 [0.52] for R_U; Tables 3 and 4). Magnitudes of uniform relief are between 130 m (Balachaur fold, Siwalik Hills) and 2645 m (Kyrgyz Range, Kyrgyzstan) with most (91%) relief measurements at <1500 m (Fig. 5B). Maximum relief magnitudes are between 172 m (Balachaur fold, Siwalik Hills) and 3567 m (Kyrgyz Range, Kyrgyzstan) with most (84%) values at <2000 m. The general trend is that slower slip and displacement rates and higher magnitudes of displacement correlate with higher relief.

Rock Strength

Our classification of lithologic strength has strong correlations with tectonic and topographic variables (R = 0.60–0.76) (Tables 3 and 4). We reiterate here that this variable is based on assumptions about rock strength and is spatially averaged over the entire analyzed mountain range. Due to the semiquantitative nature of the lithology variable, we calculated a Spearman correlation coefficient rather than a Pearson correlation coefficient, which is intended to evaluate monotonic relationships. Our analysis provides a correlation coefficient of R = 0.66 (0.60) and 0.73 (0.64) (p-value =

Geosphere, published online on 10 June 2015 as doi:10.1130/GES01156.1

≤0.001 for all, Tables 3 and 4) between lithologic strength and uniform and maximum relief, respectively. Mountains with higher relief tend to be composed of stronger (less erodible) rock. The correlation coefficient between lithologic strength and displacement is R = 0.64 (0.46), and with slip and displacement rate, it is R = –0.76 (–0.59) and R = –0.64 (–0.52) (p-value = ≤0.001 for all, Tables 3 and 4). These results suggest that substrate strength is a central control on mountain tectonomorphic systems.

DISCUSSION

What controls fault-driven topography? Landscapes are a reflection of the dynamic feedbacks between tectonics, climate, and erosion. As expected, our results do not support a single driver for landscape development, as is evident by the large scatter in our data set. That said, we do observe two constants in our data set. First, all ranges cease increasing in relief at some distance from their tips, reaching a saturation in relief within their interiors. Second, the distance over which that relief saturation is achieved is measurable as some distance from the tip ("tip zone"). Collectively, our results show significant correlations between definable topographic metrics and variables that shape the landscapes (i.e., tectonic rate, climate, and lithology). In the next section, we discuss the results of our data analysis that shed light onto dominant drivers of fault-driven landscapes, and we focus primarily on the strong, negative correlation between tip zone length and tectonic rate and the implications of that relationship for estimating the timescales of relief generation.

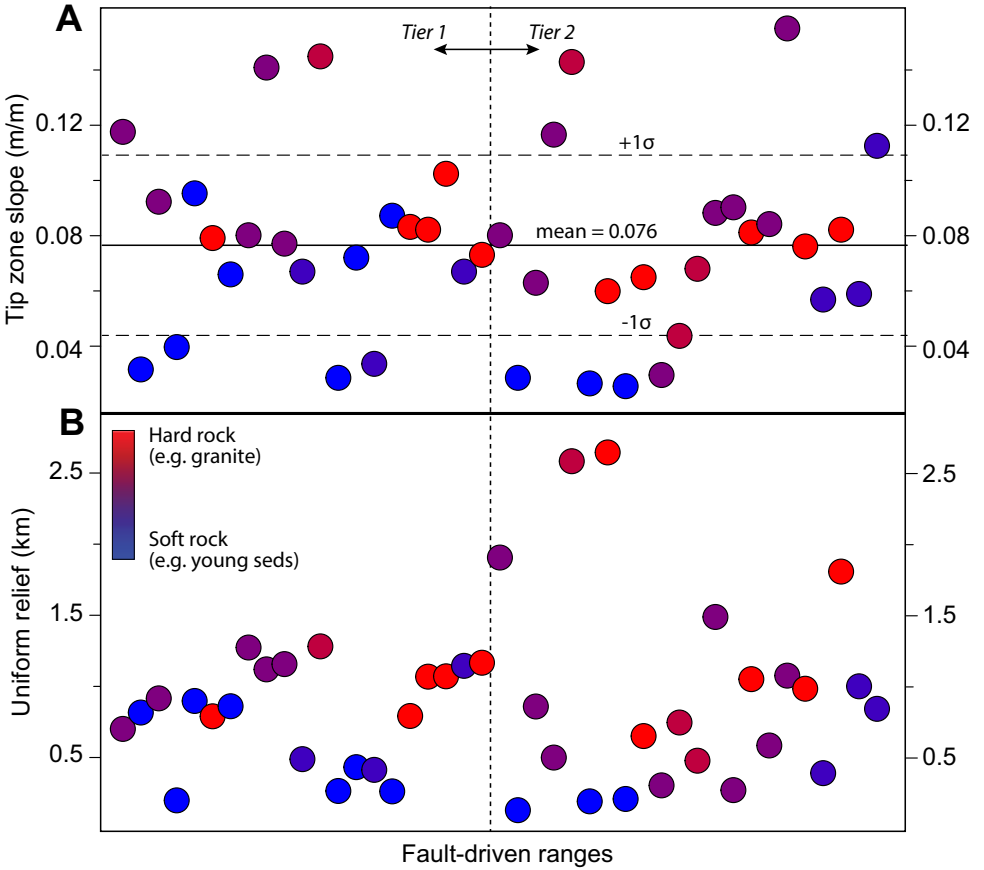

Figure 5. Trends between lithologic strength and (A) tip zone slope and (B) uniform relief. Dashed line separates Tier 1 (left) from Tier 2 (right) data. Data points are colored based on their lithologic strength data (Table 2; see text for description). Slope is shown with mean and standard deviation. Note that both tip zone slope and relief tend to increase with lithologic strength (e.g., blues change to reds).

Climate and Tectonics

The strong positive correlation between modern precipitation and tectonic rate alludes to a feedback between tectonics and climate, but whether this is a causal relationship or coincidence remains an open question. In recent decades, the role climate plays in tectonic evolution has become increasingly appreciated (e.g., Whipple, 2009) with several studies documenting the coupled increase in denudation and deformation (e.g., Willett et al., 1993; Beaumont et al., 2001; Zeitler et al., 2001; Berger et al., 2008). One way to interpret our results is as further evidence for such coupling, which suggests a universal link between rapid deformation and rainfall. A second interpretation is that the most rapidly slipping faults are at the fronts of active orogenic belts (e.g., Himalayas and Taiwan), which tend to possess high orographic precipitation. In this case, our results are simple coincidence. Regardless of the interpretation, there is an observed correlation between rapidly moving faults and the amount of regional precipitation; whether the relationship is causal, coincidence, or both remains a path for continued investigation.

Geosphere, published online on 10 June 2015 as doi:10.1130/GES01156.1

Lithology and Mountain Relief

What controls the limit to mountain relief? The morphology of all the investigated mountain ranges is characterized by increasing relief from the tip to a maximum threshold value, which we call uniform relief (R_U). The strongest correlation (with a non-topographic metric) for uniform relief of Tier 1 ranges is with displacement (R = 0.64, p-value = 0.001) and lithologic strength (R = 0.66, p-value = 0.001; Tables 3 and 4). Lithology, which we use as a proxy for substrate erodibility, has a significant influence on fault-driven landscapes. In addition to a correlation with uniform relief, lithologic strength has strong, positive monotonic relationships with maximum relief, age of onset, and displacement (Tables 3 and 4). Erosion rates are dependent on rock type, with weaker rocks displaying higher erosion rates and more mass wasting events than stronger lithologies (Schmidt and Montgomery, 1995; Molnar et al., 2007; Chen et al., 2011; Burbank and Anderson, 2012). Lithologic strength is intuitively linked with age and displacement: as uplift progresses over time, erosion removes younger, softer rocks and exposes harder, underlying rocks (Burbank et al., 1999). Thus, large-magnitude displacement tends to expose deeper, stronger rocks that decrease the erodibility of the system, which in turn results in a higher magnitude of relief. Exceptions to this generalization include crystalline intrusive bodies and thrust fault settings where older, more robust rock can be superimposed above younger, softer rock. In the absence of quantitative data on the mechanical properties of each location, this observation is somewhat speculative and presents an interesting avenue for future research. To what degree does lithology control mountain topography? Substrate properties are often impossible to compile across large areas and as a result are often overlooked in favor of tectonics or climate as dominant drivers of mountain-scale landscapes (e.g., Densmore et al., 2007b; Champagnac et al., 2012). Our results, although qualitative, suggest a significant influence of substrate strength on mountain relief.

Tip Zone Gradient and Fault Tip Taper

Our geomorphic measurements of tip zone gradient may be a reflection of underlying fault geometry, providing support for mechanical models of rock deformation. The convergence of tip zone gradient values around a mean of 0.08 (Table 2) coupled with the lack of significant trends between tip zone gradient and any other variable (Tables 3 and 4) may be indicative of critical fault tip taper (e.g., Scholz, 2002). Displacement profiles of faults show a maximum near the center of the fault and displacement tapering to zero at the tips (e.g., Fig. 1A). Fault mechanics require that displacement taper off in such a way that stresses remain finite at the tips; as slip accumulates in the fault interior, stress builds up at the fault tips until it reaches the yield strength of the rock, at which point the fault grows laterally (Cowie and Scholz, 1992c; Scholz, 2002). The angle the displacement profile forms as it tapers is called fault tip taper (FTT; Fig. 1A) and is proportional to the strength of the material (Cowie and Scholz, 1992c; Scholz et al., 1993; Scholz, 2002). Thus, based on fracture mechanics models, we would expect the tip zone slope to correlate with rock strength. The lack of correlation observed here could be because our lithology database is not very robust and/or because isolated faults grow with a constant FTT (Kanninen and Popelar, 1985; Dawers et al., 1993). If the latter, our observation that tip zone gradient values cluster between 0.07 and 0.1 may be indicative of a threshold gradient due to FTT. This speculation is further supported by the strong link between relief and tip zone length in all studied mountain ranges (R = 0.74 [0.72] for maximum relief; R = 0.70 [0.73] for uniform relief). Implicit in this observation is that if tip zone gradient converges to a threshold value, then the tip zone length and relief would have a coupled increase or decrease.

Tip Zone Length and Tectonic Rate

We find the strong correlation between deformation rates and tip zone length to be particularly interesting due to the implications for relief saturation and the temporal scales of relief growth. Why do faster deformation rates result in shorter tip zones? Assuming that the range-forming faults adhere to the well-established relationship between distance along strike and slip rate/displacement (Fig. 1), the highest slip rates will be in the along-strike center. High tectonic rates are correlated with frequent mass wasting events (Binnie et al., 2007) that contribute to rapid denudation and lower relief of mountains (Champel et al., 2002; Korup et al., 2007). If the transition from increasing to uniform relief is coincident with higher deformation rates, as predicted by conceptual models of fault growth (Fig. 1), then those higher deformation rates could in turn be coincident with more efficient erosive processes (Densmore et al., 2007b). Thus the transition to uniform relief is the landscape reflection of an erosional and tectonic balance. We can in turn speculate that temporally, ranges with faster deformation rates will experience a more rapid shift to uniform relief (i.e., shorter tip zones), especially if they consist of weak rocks in humid climates. Unfortunately, our data set for slip rates includes far more slowly moving faults (<2 km/m.y.; n = 28) than rapidly moving ones (>2 km/m.y.; n = 13; Fig. 4B and Table 1). This bias is a natural consequence of examining global fault populations; due to the processes involved in the evolution of fault populations, less active faults far outnumber highly active faults in nature (Cowie, 1998). Although the relationship between tip zone and deformation rate is strongly affected by a small number of ranges with fast deformation rates, it is the best global-scale estimate that exists.

Another possible explanation of the tip zone observations is that range relief saturation is related to seismogenic zone thickness or décollement depth. Brittle failure is limited to the uppermost portion of the crust, and the thickness varies depending on several factors including geothermal gradient, rheology, composition, and overall crustal thickness (Watts and Burov, 2003). Faults reaching the brittle-ductile transition have been evoked to explain observed maximum displacements and fault segment lengths (Scholz and Contreras, 1998); thus it may follow that tip zone length also follows a similar scaling. Shallower brittle-ductile transitions reduce the fault length, displacement, and down-dip extent of faulting (Watts and Burov, 2003); thus we would

Geosphere, published online on 10 June 2015 as doi:10.1130/GES01156.1

predict shallow décollements to be associated with shorter tip zones. The décollement beneath the Siwalik Hills at the Himalayan front is ~5–7 km (Powers et al., 1998), where short (5–6 km) measured tip zones are located (Barnes et al., 2011). In the U.S. Basin and Range, in comparison, the seismogenic zone is 15–20 km thick (Anderson et al., 1983; Stein et al., 1988), and tip zones are ~14 km long on average (9.5–20 km, Table 1). Although precise estimates for depths to décollements do not exist for many faults in our database, this example hints at a link between tip zone length and décollement depth.

It is worth mentioning that fault geometry, particularly fault-plane angle and its variation with depth, can influence the magnitude and rate of uplift and hence the resulting topography of fault-driven mountain ranges (Wickham, 1995; Hubert-Ferrari et al., 2007; Burbank and Anderson, 2012). In exerting control on rock uplift and advection, fault geometry has the potential to significantly influence mountain relief, range width, and tip zone length and gradient (Miller and Slingerland, 2006; Barnes et al., 2011; Burbank and Anderson, 2012; Styron et al., 2013). For example, in a compressional setting with ramp-flat geometry, if fault slip has overcome the vertical dimension of the ramp, then surface uplift may cease (Burbank and Anderson, 2012). The size, angle, and continuity of the ramp relative to the total slip are factors in the ratio of shortening to uplift (Suppe and Medwedeff, 1990; Hubert-Ferrari et al., 2007). It is possible that some observed tip zones are actually fault-propagation folds in transition to fault-bend folds, in which case the observed tip zone slope and length may be a combined reflection of rock properties, fault geometry, rheology, and décollement kinetics (e.g., Suppe and Medwedeff, 1990; Champel et al., 2002).

Time for Relief Generation

Our observations have implications for estimating the timescale for relief generation—in other words, the time it takes to reach a steady form, within the established fault growth framework (e.g., Fig. 1A). One idea is that the length over which uniform relief is achieved, the tip zone length, can be converted to a timescale using the fault tip propagation rate (henceforth referred to as the tip zone method), which assumes the latter is a gradual and steady process (Fig. 6A; after Densmore et al., 2004). Unfortunately, (1) few data exist on fault tip propagation rate; so it often must be estimated (here and elsewhere assumed to be ~10× the fault slip rate; e.g., Densmore et al., 2004; Barnes et al., 2011); and (2) the assumption that faults grow by systematic and simultaneous increases in both displacement and length may be inaccurate (e.g., Cowie and Scholz, 1992c; Walsh et al., 2002; Amos et al., 2010; Mouslopoulou et al., 2012). Instead, scaling properties of both earthquakes and faults support the idea that fault length may become established early on and that further growth is achieved by increases in displacement without tip propagation (Walsh et al., 2002). Due to these caveats associated with fault tip propagation, we propose another method for estimating the timescale for relief generation where the uniform relief (R_U) is divided by the long-term displacement rate (henceforth referred to as the uniform relief [R_U] method; Fig. 6B). R_U represents the mean relief accumulated in response to active faulting combined with the evolving erosional processes that shape the uplifting landscape. Thus, dividing R_U by the long-term displacement rate provides an estimate for the minimum amount of time required to accumulate the relief because presumably the range crest itself has lowered some due to erosion. Both methods discussed here produce similar estimates for the timescale to reach steady relief (Fig. 6C). That said, we favor the uniform relief method because estimating fault tip propagation rate using a 10:1 ratio to fault slip rate is based on theory with limited supporting data (Morewood and Roberts, 1999), whereas displacement rate is more likely to be independently constrained.

Applying the uniform relief method provides timescales to reach steady relief varying from ~30 k.y. to 4 m.y. for the Tier 1 ranges (Fig. 6B). What does it mean when range topography reaches a steady form? We suggest that beyond time periods greater than those required to achieve uniform relief, the range begins acting as a tectonically and geomorphically coherent system. Upon reaching this evolved phase of development, fault-

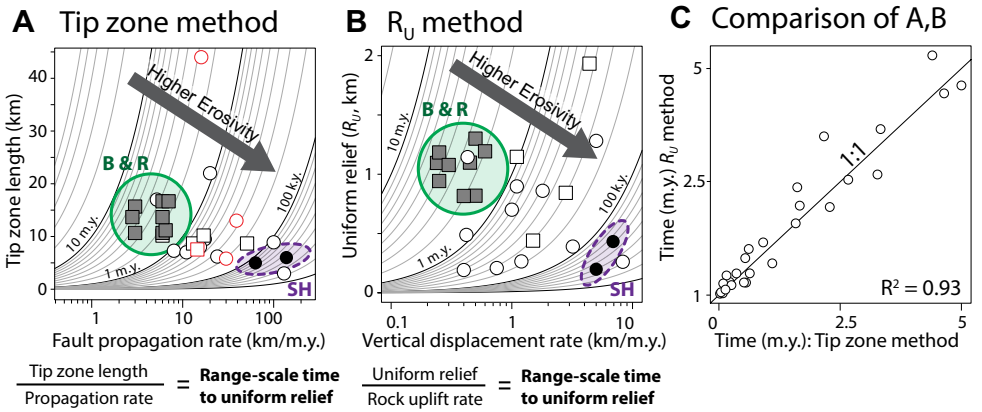

Figure 6. Quantifying timescales to reach uniform relief in emergent ranges. Tier 1 data and data for ranges with independently constrained propagation rates (red symbols in A) are included. (A) Tip zone method: tip zone versus propagation rate, estimated using 10:1 ratio between tip propagation and slip rate (after Densmore et al., 2004). Red circles are ranges with independently measured propagation rates: Kyrgyz Range, S. Alkyonides fault, Kashi anticline, and Wheeler Range (see Notes section in the Supplemental File [see footnote 1]). Curves are contours of the time required for the fault to propagate across the tip zone length. (B) R_U method: mean uniform relief (R_U) versus rock uplift rate. Curves are contours of the time required for the range to reach uniform relief. Squares—normal faults; circles—reverse faults; filled squares—Basin and Range (B & R); filled circles—Siwalik Hills (SH). (C) Comparison of time needed to reach steady relief between the two methods.

Geosphere, published online on 10 June 2015 as doi:10.1130/GES01156.1

driven ranges are in equilibrium with their regional tectonomorphic setting. For example, ranges within the same tectonic province, with similar size, slip rate, and climate, require similar timescales to reach a steady form. The nine (Tier 1) faults in our database from the U.S. Basin and Range are estimated to take between 1 and 5 m.y. to saturate in relief (green circle, Fig. 6); the two (Tier 1) faults from the Siwalik Hills take between 30 and 70 k.y. (purple oval, Fig. 6). Our results are consistent with landscape evolution models that predict steady-state topography in the Basin and Range takes ~1–4 m.y. to develop (Ellis et al., 1999). Basin and Range faults have longer tip zones, greater relief, slower slip rates, and lower rates of precipitation than Siwalik Hills faults (Fig. 6; Tables 1 and 2), resulting in overall lower erosivity in the Basin and Range. Our findings suggest that emergent ranges uplifting due to active faults display regionally consistent self-similar forms that reflect their particular environmental balance between tectonic input and erosional output similar to what other studies have shown at orogenic-belt scales (e.g., Willett and Brandon, 2002; Champagnac et al., 2012). The implication is that distinctive, identifiable equilibrium landscape forms may be used to estimate the timescale for their development.

Predicting Faulting Rate from Topography?

Our data analysis also suggests we can predict first-order fault kinematics from emergent topography in places where faulting rate estimates do not exist. Learning how to exploit landscape form to unravel tectonics remains an overarching goal of tectonic geomorphologic research (e.g., Kirby et al., 2003; Wobus et al., 2006; Boulton and Whittaker, 2009). For example, little is known about displacement or slip rates in the seismically active region of Iran's border with Afghanistan and Pakistan (Walker and Jackson, 2004). One thrust fault tip zone in the Makran Region measured 7.7 ± 0.8 km long (blue diamond, Fig. 2). Using the relationship between displacement rate and tip zone length from our analysis, this tip zone implies a displacement rate of 4.6 ± 0.7 km/m.y. and a slip rate of 8.1 ± 1.4 km/m.y. (yellow diamond, Figs. 4A and 4B). This estimate is consistent with sparse geomorphic and global positioning system (GPS) evidence that estimates regional slip rates are between 2.5 and 6 mm/yr (Walker and Jackson, 2004). For mountain ranges with long tip zones (>15 km), the potential to predict the deformation rate with precision is somewhat limited based on the scatter in our data set. While caution should be noted, the data and relationships presented here have the power to provide (1) a starting point for more thorough study or (2) an estimate for a remote location where thorough investigation is difficult.

CONCLUSIONS

Our global analysis of tectonomorphic variables from active fault-driven ranges shows that emergent ranges always achieve uniform relief, and the spatiotemporal scales over which this steady form is achieved correlate with the long-term ($10^{4–6}$ yr) fault slip and displacement rate. In short, rapidly slipping faults produce mountain ranges that saturate in relief over shorter distances and in less time than slowly slipping faults. Furthermore, maximum mountain relief has stronger correlations with lithology and total fault displacement than displacement rate. Our results (1) imply that there are broad tectonic controls on the early phases of topographic growth that can be modulated by regional variations in lithology and climate; (2) warn that the impacts of climate and lithology on mountain relief should not be ignored; and (3) suggest that relief patterns in uplifting landscapes may be used as a first-order predictor of faulting rate. Our results may provide further insights into basic links between tectonics, topography, and climate when compared with data from other scales.

ACKNOWLEDGMENTS

M. Ellis thanks the University of North Carolina Department of Geological Sciences Martin Fund, Geological Society of America, and Sigma Xi for financial support. James Spotila, Dylan Ward, Patience Cowie, Nancye Dawers, Mike Taylor, Associate Editor Colin Amos, and an anonymous reviewer provided many helpful comments that helped improve this paper.

REFERENCES CITED

Adams, K.K., and Sawyer, T.L., 1999, Fault number 1635, Western Humboldt Range fault zone: Quaternary fault and fold database of the United States, U.S. Geological Survey website, http://earthquakes.usgs.gov/hazards/qfaults, May, 2012.

Ahnert, F., 1970, Functional relationships between denudation, relief, and uplift in large, mid-latitude drainage basins: American Journal of Science, v. 268, no. 3, p. 243–263, doi:10.2475/ajs.268.3.243.

Allen, M., Jackson, J., and Walker, R., 2004, Late Cenozoic reorganization of the Arabia-Eurasia collision and the comparison of short-term and long-term deformation rates: Tectonics, v. 23, no. 2, doi:10.1029/2003TC001530.

Amos, C.B., Burbank, D.W., Nobes, D.C., and Read, S.A.L., 2007, Geomorphic constraints on listric thrust faulting: Implications for active deformation in the Mackenzie Basin, South Island, New Zealand: Journal of Geophysical Research: Solid Earth, v. 112, no. B3, p. 1–24, doi:10.1029/2006jb004291.

Amos, C.B., Burbank, D.W., and Read, S.A.L., 2010, Along-strike growth of the Ostler fault, New Zealand: Consequences for drainage deflection above active thrusts: Tectonics, v. 29, no. 4, doi:10.1029/2009TC002613.

Anders, M.H., Spiegelman, M., Rodgers, D.W., and Hagstrum, J.T., 1993, The growth of fault-bounded tilt blocks: Tectonics, v. 12, no. 6, p. 1451–1459, doi:10.1029/93TC01547.

Anderson, E., 1905, The dynamics of faulting: Transactions of the Edinburgh Geological Society, v. 8, no. 3, p. 387–402, doi:10.1144/transed.8.3.387.

Anderson, R.E., Zoback, M., and Thompson, G.A., 1983, Implications of selected subsurface data on the structural form and evolution of some basins in the northern Basin and Range province, Nevada and Utah: Geological Society of America Bulletin, v. 94, no. 9, p. 1055–1072, doi:10.1130/0016-7606(1983)94<1055:IOSSDO>2.0.CO;2.

Armijo, R., Meyer, B., King, G.C.P., and Papanastassiou, D., 1996, Quaternary evolution of the Corinth Rift and its implications for the Late Cenozoic evolution of the Aegean: Geophysical Journal International, v. 126, no. 1, p. 11–53, doi:10.1111/j.1365-246X.1996.tb05264.x.

Avdeev, B., and Niemi, N.A., 2011, Rapid Pliocene exhumation of the central Greater Caucasus constrained by low-temperature thermochronometry: Tectonics, v. 30, no. 2, doi:10.1029/2010TC002808.

Balestrieri, M.L., Moratti, G., Bigazzi, G., and Algouti, A., 2009, Neogene exhumation of the Marrakech High Atlas (Morocco) recorded by apatite fission-track analysis: Terra Nova, v. 21, no. 2, p. 75–82, doi:10.1111/j.1365-3121.2008.00857.x.

Barnes, J.B., Densmore, A.L., Mukul, M., Sinha, R., Jain, V., and Tandon, S.K., 2011, Interplay between faulting and base level in the development of Himalayan frontal fold topography: Journal of Geophysical Research, v. 116, no.F3, doi:10.1029/2010JF001841.

Beaumont, C., Jamieson, R.A., Nguyen, M.H., and Lee, B., 2001, Himalayan tectonics explained by extrusion of a low-viscosity crustal channel coupled to focused surface denudation: Nature, v. 414, no. 6865, p. 738–742, doi:10.1038/414738a.

Becker, A., Finger, P., Meyer-Christoffer, A., Rudolf, B., Schamm, K., Schneider, U., and Ziese, M., 2013, A description of the

Geosphere, published online on 10 June 2015 as doi:10.1130/GES01156.1

global land-surface precipitation data products of the Global Precipitation Climatology Centre with sample applications including centennial (trend) analysis from 1901–present: Earth System Science Data, v. 5, no. 1, p. 71–99, doi:10.5194/essd-5-71-2013.

Benedetti, L., Tapponnier, P., King, G.C.P., Meyer, B., and Manighetti, I., 2000, Growth folding and active thrusting in the Montello region, Veneto, northern Italy: Journal of Geophysical Research, v. 105, p. 739–766, doi:10.1029/1999JB900222.

Bennett, E., Youngson, J., Jackson, J., Norris, R., Raisbeck, G., and Yiou, F., 2006, Combining geomorphic observations with in situ cosmogenic isotope measurements to study anticline growth and fault propagation in Central Otago, New Zealand: New Zealand Journal of Geology and Geophysics, v. 49, p. 217–231, doi:10.1080/00288306.2006.9515161.

Berger, A.L., Gulick, S.P.S., Spotila, J.A., Upton, P., Jaeger, J.M., Chapman, J.B., Worthington, L.A., Pavlis, T.L., Ridgway, K.D., Willems, B.A., and McAleer, R.J., 2008, Quaternary tectonic response to intensified glacial erosion in an orogenic wedge: Nature Geoscience, v. 1, no. 11, p. 793–799, doi:10.1038/ngeo334.

Berryman, K., Villamor, P., Nairn, I., van Dissen, R., Begg, J., and Lee, J., 2008, Late Pleistocene surface rupture history of the Paeroa fault, Taupo Rift, New Zealand: New Zealand Journal of Geology and Geophysics, v. 51, no. 2, p. 135–158, doi:10.1080/00288300809509855.

Binnie, S.A., Phillips, W.M., Summerfield, M.A., and Fifield, L.K., 2007, Tectonic uplift, threshold hillslopes, and denudation rates in a developing mountain range: Geology, v. 35, no. 8, p. 743–746, doi:10.1130/g23641a.1.

Blanc, E.J.P., Allen, M.B., Inger, S., and Hassani, H., 2003, Structural styles in the Zagros Simple Folded Zone, Iran: Journal of the Geological Society of London, v. 160, no. 3, p. 401–412, doi:10.1144/0016-764902-110.

Boulton, S.J., and Whittaker, A.C., 2009, Quantifying the slip rates, spatial distribution and evolution of active normal faults from geomorphic analysis: Field examples from an oblique-extensional graben, southern Turkey: Geomorphology, v. 104, no. 3–4, p. 299–316, doi:10.1016/j.geomorph.2008.09.007.

Bullen, M.E., Burbank, D.W., and Garver, J.L., 2003, Building the Northern Tien Shan: Integrating thermal, structural, and topographic constraints: The Journal of Geology, v. 111, p. 149–165, doi:10.1086/345840.

Burbank, D.W., and Anderson, R.S., 2012, Tectonic Geomorphology, 2nd edition: West Sussex, UK, Wiley-Blackwell.

Burbank, D.W., McLean, J.K., Bullen, M., Abdrakhmatov, K.Y., and Miller, M.M., 1999, Partitioning of intermontane basins by thrust-related folding, Tien Shan, Kyrgyzstan: Basin Research, v. 11, no. 1, p. 75–92, doi:10.1046/j.1365-2117.1999.00086.x.

Carretier, S., Regard, V., Vassallo, R., Aguilar, G., Martinod, J., Riquelme, R., Pepin, E., Charrier, R., Hérail, G., Farías, M., Guyot, J.-L., Vargas, G., and Lagane, C., 2013, Slope and climate variability control of erosion in the Andes of central Chile: Geology, v. 41, no. 2, p. 195–198, doi:10.1130/G33735.1.

Champagnac, J.-D., Molnar, P., Sue, C., and Herman, F., 2012, Tectonics, climate, and mountain topography: Journal of Geophysical Research: Solid Earth, v. 117, no. B2, p. 1–34, doi:10.1029/2011jb008348.

Champel, B., van der Beek, P., Mugnier, J.-L., and Leturmy, P., 2002, Growth and lateral propagation of fault-related folds in the Siwaliks of western Nepal: Rates, mechanisms, and geomorphic signature: Journal of Geophysical Research: Solid Earth, v. 107, no. B6, p. ETG 2-1–ETG 2-18, doi:10.1029/2001JB000578.

Chen, H., Lin, G.-W., Lu, M.-H., Shih, T.-Y., Horng, M.-J., Wu, S.-J., and Chuang, B., 2011, Effects of topography, lithology, rainfall and earthquake on landslide and sediment discharge in mountain catchments of southeastern Taiwan: Geomorphology, v. 133, no. 3–4, p. 132–142, doi:10.1016/j.geomorph.2010.12.031.

Chen, J., Heermance, R., Burbank, D.W., Scharer, K.M., Miao, J., and Wang, C., 2007, Quantification of growth and lateral propagation of the Kashi anticline, southwest Chinese Tian Shan: Journal of Geophysical Research: Solid Earth, v. 112, no. B3, p. 1–22, doi:10.1029/2006jb004345.

Colgan, J.P., Dumitru, T.A., Reiners, P.W., Wooden, J.L., and Miller, E.L., 2006, Cenozoic Tectonic Evolution of the Basin and Range Province in Northwestern Nevada: American Journal of Science, v. 306, no. 8, p. 616–654, doi:10.2475/08.2006.02.

Colgan, J.P., Howard, K.A., Fleck, R.J., and Wooden, J.L., 2010, Rapid middle Miocene extension and unroofing of the southern Ruby Mountains, Nevada: Tectonics, v. 29, no. 6, doi:10.1029/2009TC002655.

Cowgill, E., Arrowsmith, J.R., Yin, A., Wang, X., and Chen, Z., 2004, The Akato Tagh bend along the Altyn Tagh fault, northwest Tibet 2: Active deformation and the importance of transpression and strain hardening within the Altyn Tagh system: Geological Society of America Bulletin, v. 116, no. 11–12, p. 1443–1464, doi:10.1130/B25360.1.

Cowie, P.A., 1998, A healing-reloading feedback control on the growth rate of seismogenic faults: Journal of Structural Geology, v. 20, no. 8, p. 1075–1087, doi:10.1016/S0191-8141(98)00034-0.

Cowie, P.A., and Roberts, G.P., 2001, Constraining slip rates and spacings for active normal faults: Journal of Structural Geology, v. 23, no. 12, p. 1901–1915, doi:10.1016/S0191-8141(01)00036-0.

Cowie, P.A., and Scholz, C.H., 1992a, Displacement-length scaling relationship for faults: Data synthesis and discussion: Journal of Structural Geology, v. 14, no. 10, p. 1149–1156, doi:10.1016/0191-8141(92)90066-6.

Cowie, P.A., and Scholz, C.H., 1992b, Growth of Faults by Accumulation of Seismic Slip: Journal of Geophysical Research, v. 97, no. B7, p. 11,085–11,095, doi:10.1029/92JB00586.

Cowie, P.A., and Scholz, C.H., 1992c, Physical explanation for the displacement-length relationship of faults using a post-yield fracture mechanics model: Journal of Structural Geology, v. 14, no. 10, p. 1133–1148, doi:10.1016/0191-8141(92)90065-5.

Cowie, P.A., and Shipton, Z.K., 1998, Fault tip displacement gradients and process zone dimensions: Journal of Structural Geology, v. 20, no. 8, p. 983–997, doi:10.1016/S0191-8141(98)00029-7.

Dahlen, F.A., and Suppe, J., 1988, Mechanics, growth, and erosion of mountain belts, *in* Clark, S.P., Jr., Burchfiel, B.C., and Suppe, J., eds., Processes in Continental Lithospheric Deformation: Boulder, Colorado, Geological Society of America Special Paper 218, p. 161–178.

Davis, J.C., 2002, Statistics and Data Analysis in Geology, 3rd Edition: John Wiley and Sons.

Davis, K., Burbank, D.W., Fisher, D., Wallace, S., and Nobes, D., 2005, Thrust-fault growth and segment linkage in the active Ostler fault zone, New Zealand: Journal of Structural Geology, v. 27, no. 8, p. 1528–1546, doi:10.1016/j.jsg.2005.04.011.

Dawers, N.H., and Anders, M.H., 1995, Displacement-length scaling and fault linkage: Journal of Structural Geology, v. 17, no. 5, p. 607–614, doi:10.1016/0191-8141(94)00091-D.

Dawers, N.H., Anders, M.H., and Scholz, C.H., 1993, Growth of normal faults: Displacement-length scaling: Geology, v. 21, no. 12, p. 1107–1110, doi:10.1130/0091-7613(1993)021<1107:GONFDL>2.3.CO;2.

Densmore, A.L., Dawers, N.H., Gupta, S., Guidon, R., and Goldin, T., 2004, Footwall topographic development during continental extension: Journal of Geophysical Research, v. 109, doi:10.1029/2003JF000115.

Densmore, A.L., Allen, P.A., and Simpson, G., 2007a, Development and response of a coupled catchment fan system under changing tectonic and climatic forcing: Journal of Geophysical Research, v. 112, no. F1, doi:10.1029/2006JF000474.

Densmore, A.L., Gupta, S., Allen, P.A., and Dawers, N.H., 2007b, Transient landscapes at fault tips: Journal of Geophysical Research, v. 112, doi:10.1029/2006JF000560.

Echavarria, L., Hernandez, R., Allmendinger, R., and Reynolds, J., 2003, Subandean thrust and fold belt of northwestern Argentina: Geometry and timing of the Andean evolution: The American Association of Petroleum Geologists Bulletin, v. 87, no. 6, p. 965–985, doi:10.1306/01200300196.

Ellis, M.A., Densmore, A.L., and Anderson, R.S., 1999, Development of mountainous topography in the Basin and Ranges, USA: Basin Research, v. 11, no. 1, p. 21–41, doi:10.1046/j.1365-2117.1999.00087.x.

Espurt, N., Barbarand, J., Roddaz, M., Brusset, S., Baby, P., Saillard, M., and Hermoza, W., 2011, A scenario for late Neogene Andean shortening transfer in the Camisea Subandean zone (Peru, 12°S): Implications for growth of the northern Andean Plateau: Geological Society of America Bulletin, v. 123, no. 9–10, p. 2050–2068, doi:10.1130/B30165.1.

Forte, A.M., Cowgill, E., Bernardin, T., Kreylos, O., and Hamann, B., 2010, Late Cenozoic deformation of the Kura fold-thrust belt, southern Greater Caucasus: Geological Society of America Bulletin, v. 122, no. 3/4, p. 465–486, doi:10.1130/b26464.1.

Friedrich, A.M., Wernicke, B.P., Niemi, N.A., Bennett, R.A., and Davis, J.L., 2003, Comparison of geodetic and geologic data from the Wasatch region, Utah, and implications for the spectral character of Earth deformation at periods of 10 to 10 million years: Journal of Geophysical Research, v. 108, no. B4, p. 7-1–7-23, doi:10.1029/2001JB000682.

Fuller, C.W., Willett, S.D., Fisher, D., and Lu, C.Y., 2006, A thermomechanical wedge model of Taiwan constrained by fission-track thermochronometry: Tectonophysics, v. 425, no. 1–4, p. 1–24, doi:10.1016/j.tecto.2006.05.018.

Ghisetti, F.C., Gorman, A.R., and Sibson, R.H., 2007, Surface breakthrough of a basement fault by repeated seismic slip episodes: The Ostler fault, South Island, New Zealand: Tectonics, v. 26, no. 6, doi:10.1029/2007TC002146.

Gold, R.D., Cowgill, E., Wang, X.-F., and Chen, X.-H., 2006, Application of trishear fault-propagation folding to active reverse faults: Examples from the Dalong fault, Gansu

Geosphere, published online on 10 June 2015 as doi:10.1130/GES01156.1

Province, NW China: Journal of Structural Geology, v. 28, no. 2, p. 200–219, doi:10.1016/j.jsg.2005.10.006.

Gorynski, K.E., Stockli, D.F., and Walker, J.D., 2013, Thermochronometrically constrained anatomy and evolution of a Miocene extensional accommodation zone and tilt domain boundary: The southern Wassuk Range, Nevada: Tectonics, v. 32, no. 3, p. 516–539, doi:10.1002/tect.20044.

Gupta, A., and Scholz, C.H., 2000, A model of normal fault interaction based on observations and theory: Journal of Structural Geology, v. 22, no. 7, p. 865–879, doi:10.1016/S0191-8141(00)00011-0.

Guzofski, C.A., Shaw, J.H., Lin, G., and Shearer, P.M., 2007, Seismically active wedge structure beneath the Coalinga anticline, San Joaquin basin, California: Journal of Geophysical Research: Solid Earth, v. 112, no. B3, p. 1–14, doi:10.1029/2006jb004465.

Harbor, D.J., 1997, Landscape evolution at the margin of the Basin and Range: Geology, v. 25, no. 12, p. 1111–1114, doi:10.1130/0091-7613(1997)025<1111:LEATMO>2.3.CO;2.

Homke, S., Verges, J., Garces, M., Emami, H., and Karpuz, R., 2004, Magnetostratigraphy of Miocene–Pliocene Zagros foreland deposits in the front of the Push-e Kush Arc (Lurestan Province, Iran): Earth and Planetary Science Letters, v. 225, no. 3–4, p. 397–410, doi:10.1016/j.epsl.2004.07.002.

Hubert-Ferrari, A., Suppe, J., Gonzalez-Mieres, R., and Wang, X., 2007, Mechanisms of active folding of the landscape (southern Tian Shan, China): Journal of Geophysical Research: Solid Earth, v. 112, no. B3, p. 1–39, doi:10.1029/2006jb004362.

Janecke, S.U., Geissman, J.W., and Bruhn, R.L., 1991, Localized rotation during Paleogene Extension in east central Idaho: Paleomagnetic and geologic evidence: Tectonics, v. 10, no. 2, p. 403–432, doi:10.1029/90TC02465.

Kanninen, M.F., and Popelar, C.H., 1985, Advanced Fracture Mechanics: Oxford, Oxford University Press.

Keller, E.A., Zepeda, R.L., Rockwell, T.K., Ku, T.L., and Dinklage, W.S., 1998, Active tectonics at Wheeler Ridge, southern San Joaquin Valley, California: Geological Society of America Bulletin, v. 110, no. 3, p. 298–310, doi:10.1130/0016-7606(1998)110<0298:ATAWRS>2.3.CO;2.

Kirby, E., Whipple, K.X., Wenqing, T., and Zhiliang, C., 2003, Distribution of active rock uplift along the eastern margin of the Tibetan Plateau: Inferences from bedrock channel longitudinal profiles: Journal of Geophysical Research: Solid Earth, v. 108, no. B4, p. 16–1–16–24, doi:10.1029/2001JB000861.

Korup, O., Clague, J.J., Hermanns, R.L., Hewitt, K., Strom, A.L., and Weidinger, J.T., 2007, Giant landslides, topography, and erosion: Earth and Planetary Science Letters, v. 261, no. 3–4, p. 578–589, doi:10.1016/j.epsl.2007.07.025.

Kottek, M., Grieser, J., Beck, C., Rudolf, B., and Rubel, F., 2006, World Map of the Koppen-Geiger climate classification updated: Meteorologische Zeitschrift, v. 15, no. 3, p. 259–263, doi:10.1127/0941-2948/2006/0130.

Malik, J.N., and Nakata, T., 2003, Active faults and related Late Quaternary deformation along the Northwestern Himalayan Frontal Zone, India: Annals of Geophysics, v. 46, no. 5, p. 917–936.

Markley, M., and Norris, R.J., 1999, Structure and neotectonics of the Blackstone Hill Antiform, Central Otago, New Zealand: New Zealand Journal of Geology and Geophysics, v. 42, p. 205–218, doi:10.1080/00288306.1999.9514840.

McLeod, A.E., Dawers, N.H., and Underhill, J.R., 2000, The propagation and linkage of normal faults: Insights from the Strathspey-Brent-Statfjord fault array, northern North Sea: Basin Research, v. 12, no. 3–4, p. 263–284, doi:10.1111/j.1365-2117.2000.00124.x.

Medwedeff, D., 1992, Geometry and kinematics of an active, laterally propagating wedge thrust, Wheeler Ridge, California, *in* Mitra, S., and Fisher, G., eds., Structural Geology of Fold and Thrust Belts: Baltimore, Maryland, Johns Hopkins University Press, p. 3–28.

METI (Ministry of Economy, Trade, and Industry) and NASA (National Aeronautics and Space Administration), 2012, Advanced Spaceborne Thermal Emission and Reflection Radiometer (ASTER) Global Digital Elevation Model (GDEM), Version 2: Sioux Falls, South Dakota, Earth Observing System (EOS) Data Information System (EOSDIS) Land Processes (LP) Distributed Active Archive Center (DAAC).

Miller, S.R., and Slingerland, R.L., 2006, Topographic advection on fault-bend folds: Inheritance of valley positions and the formation of wind gaps: Geology, v. 34, no. 9, p. 769–772, doi:10.1130/G22658.1.

Molnar, P., Anderson, R.S., and Anderson, S.P., 2007, Tectonics, fracturing of rock, and erosion: Journal of Geophysical Research: Earth Surface, v. 112, no. F3, p. 1–12, doi:10.1029/2005jf000433.

Montgomery, D.R., and Brandon, M.T., 2002, Topographic controls on erosion rates in tectonically active mountain ranges: Earth and Planetary Science Letters, v. 201, no. 3–4, p. 481–489, doi:10.1016/S0012-821X(02)00725-2.

Montgomery, D.R., Balco, G., and Willett, S.D., 2001, Climate, tectonics, and the morphology of the Andes: Geology, v. 29, no. 7, p. 579–582, doi:10.1130/0091-7613(2001)029<0579:ctatmo>2.0.co;2.

Morewood, N.C., and Roberts, G.P., 1999, Lateral propagation of the surface trace of the South Alkyonides normal fault segment, central Greece: Its impact on models of fault growth and displacement-length relationships: Journal of Structural Geology, v. 21, no. 6, p. 635–652, doi:10.1016/S0191-8141(99)00049-8.

Mosar, J., Kangarli, T., Bochud, M., Glasmacher, U.A., Rast, A., Brunet, M.-F., and Sosson, M., 2010, Cenozoic–Recent tectonics and uplift in the Greater Caucasus: A perspective from Azerbaijan: Geological Society of London, Special Publications, v. 340, p. 261–280, doi:10.1144/SP340.12.

Mouslopoulou, V., Walsh, J.J., and Nicol, A., 2009, Fault displacement rates on a range of timescales: Earth and Planetary Science Letters, v. 278, no. 3–4, p. 186–197, doi:10.1016/j.epsl.2008.11.031.

Mouslopoulou, V., Nicol, A., Walsh, J.J., Begg, J.G., Townsend, D.B., and Hristopulos, D.T., 2012, Fault-slip accumulation in an active rift over thousands to millions of years and the importance of paleoearthquake sampling: Journal of Structural Geology, v. 36, p. 71–80, doi:10.1016/j.jsg.2011.11.010.

Namson, J.S., and Davis, T.L., 1988, Seismically active fold and thrust belt in the San Joaquin Valley, central California: Geological Society of America Bulletin, v. 100, no. 2, p. 257–273, doi:10.1130/0016-7606(1988)100<0257:SAFATB>2.3.CO;2.

Nicol, A., Walsh, J., Berryman, K., and Villamor, P., 2006, Interdependence of fault displacement rates and paleoearthquakes in an active rift: Geology, v. 34, no. 10, p. 865–868, doi:10.1130/G22335.1.

Obert, L., and Duvall, W.I., 1967, Rock mechanics and the design of structures in rock: New York, John Wiley and Sons, Inc.

Oswald, J.A., Sawyer, T.L., Rowley, P.C., and Anderson, R.E., 1998, Fault number 1590, Pilot Creek Valley fault: Quaternary fault and fold database of the United States, U.S. Geological Survey website, http://earthquakes.usgs.gov/hazards/qfaults, May, 2012.

Oveisi, B., Lavé, J., and Beek, P., 2007, Rates and Processes of Active Folding Evidenced by Pleistocene Terraces at the Central Zagros Front (Iran), *in* Lacombe, O., Roure, F., Lavé, J., and Vergés, J., eds., Thrust Belts and Foreland Basins: Berlin Heidelberg, Springer, p. 267–287.

Pavlis, T.L., Rutkofske, J., Guerrero, F., and Serpa, L.F., 2014, Structural overprinting of Mesozoic thrust systems in eastern California and its importance to reconstruction of Neogene extension in the southern Basin and Range: Geosphere, v. 10, no. 4, p. 732–756, doi:10.1130/GES00993.1.

Pinet, P., and Souriau, M., 1988, Continental erosion and large-scale relief: Tectonics, v. 7, no. 3, p. 563–582, doi:10.1029/TC007i003p00563.

Powers, P.M., Lillie, R.J., and Yeats, R.S., 1998, Structure and shortening of the Kangra and Dehra Dun reentrants, Sub-Himalaya, India: Geological Society of America Bulletin, v. 110, no. 8, p. 1010–1027, doi:10.1130/0016-7606(1998)110<1010:SASOTK>2.3.CO;2.

Ramsey, L.A., Walker, R.T., and Jackson, J., 2008, Fold evolution and drainage development in the Zagros Mountains of Fars Province, SE Iran: Basin Research, v. 20, no. 1, p. 23–48, doi:10.1111/j.1365-2117.2007.00342.x.

Redsteer, M.H., and Lidke, D.J., 1998, Fault number 1337, Toiyabe Range fault zone: Quaternary fault and fold database of the United States, U.S. Geological Survey website, http://earthquakes.usgs.gov/hazards/qfaults, March, 2015.

Redsteer, M.H., and Machette, M.N., 2000, Fault number 1212, Diamond Mountains fault zone: Quaternary fault and fold database of the United States, U.S. Geological Survey website, http://earthquakes.usgs.gov/hazards/qfaults, May, 2012.

Roberts, G.P., and Michetti, A.M., 2004, Spatial and temporal variations in growth rates along active normal fault systems: An example from the Lazio-Abruzzo Apennines, central Italy: Journal of Structural Geology, v. 26, no. 2, p. 339–376, doi:10.1016/S0191-8141(03)00103-2.

Roberts, G.P., Cowie, P., Papanikolaou, I., and Michetti, A.M., 2004, Fault scaling relationships, deformation rates and seismic hazards: An example from the Lazio-Abruzzo Apennines, central Italy: Journal of Structural Geology, v. 26, no. 2, p. 377–398, doi:10.1016/S0191-8141(03)00104-4.

Scharer, K.M., Burbank, D.W., Chen, J., and Weldon, R.J., 2006, Kinematic models of fluvial terraces over active detachment folds: Constraints on the growth mechanism of the Kashi-Atushi fold system, Chinese Tian Shan: Geological Society of America Bulletin, v. 118, no. 7–8, p. 1006–1021, doi:10.1130/B25835.1.

Schlische, R.W., Young, S.S., Ackermann, R.V., and Gupta, A., 1996, Geometry and scaling relations of a population of very small rift-related normal faults: Geology, v. 24, no. 8, p. 683–686, doi:10.1130/0091-7613(1996)024<0683:GASROA>2.3.CO;2.

Schmidt, K.M., and Montgomery, D.R., 1995, Limits to relief: Science, v. 270, no. 5236, p. 617–620, doi:10.1126/science.270.5236.617.

Geosphere, published online on 10 June 2015 as doi:10.1130/GES01156.1

Schneider, U., Becker, A., Finger, P., Meyer-Christoffer, A., Ziese, M., and Rudolf, B., 2014, GPCC's new land surface precipitation climatology based on quality-controlled in situ data and its role in quantifying the global water cycle: Theoretical and Applied Climatology, v. 115, no. 1–2, p. 15–40, doi: 10.1007/s00704-013-0860-x.

Scholz, C.H., 2002, The Mechanics of Earthquakes and Faulting, 2nd edition: Cambridge University Press.

Scholz, C.H., and Contreras, J.C., 1998, Mechanics of continental rift architecture: Geology, v. 26, no. 11, p. 967–970, doi:10.1130/0091-7613(1998)026<0967:MOCRA>2.3.CO;2.

Scholz, C.H., Dawers, N.H., Yu, J.Z., and Anders, M.H., 1993, Fault growth and fault scaling laws: Preliminary results: Journal of Geophysical Research: Solid Earth, v. 98, no. B12, p. 21,951–21,961, doi:10.1029/93JB01008.

Simoes, M., Avouac, J.P., Beyssac, O., Goffe, B., Farley, K.A., and Chen, Y.G., 2007, Mountain building in Taiwan: A thermokinematic model: Journal of Geophysical Research: Solid Earth, v. 112, no. B11, doi:10.1029/2006jb004824.

Sobel, E.R., Oskin, M., Burbank, D., and Mikolaichuk, A., 2006, Exhumation of basement-cored uplifts: Example of the Kyrgyz Range quantified with apatite fission track thermochronology: Tectonics, v. 25, doi:10.1029/2005TC001809.

Spearman, C., 1904, The proof and measurement of association between two things: The American Journal of Psychology, v. 15, no. 1, p. 72–101, doi:10.2307/1412159.

Stein, R.S., King, G.C.P., and Rundle, J.B., 1988, The growth of geological structures by repeated earthquakes 2. Field examples of continental dip-slip faults: Journal of Geophysical Research: Solid Earth, v. 93, no. B11, p. 13,319–13,331, doi:10.1029/JB093iB11p13319.

Stockli, D.F., 1999, Regional timing and spatial distribution of Miocene extension in the northern Basin and Range Province [Ph.D. thesis]: Stanford University, 239 p.

Stockli, D.F., Surpless, B.E., Dumitru, T.A., and Farley, K., 2002, Thermochronological constraints on the timing and magnitude of Miocene and Pliocene extension in the central Wassuk Range, western Nevada: Tectonics, v. 21, no. 4, p. 10-1–10-19, doi:10.1029/2001TC001295.

Stockli, D.F., Dumitru, T.A., McWilliams, M.O., and Farley, K.A., 2003, Cenozoic tectonic evolution of the White Mountains, California and Nevada: Geological Society of America Bulletin, v. 115, no. 7, p. 788–816, doi:10.1130/0016-7606(2003)115<0788:CTEOTW>2.0.CO;2.

Stolar, D.B., Willett, S.D., and Roe, G.H., 2006, Climatic and tectonic forcing of a critical orogen, *in* Willett, S.D., Hovius, N., Brandon, M.T., and Fisher, D.M., eds., Tectonics, Climate, and Landscape Evolution: Boulder, Colorado, Geological Society of America Special Paper 398, p. 241–250.

Stolar, D.B., Willett, S.D., and Montgomery, D.R., 2007, Characterization of topographic steady state in Taiwan: Earth and Planetary Science Letters, v. 261, no. 3–4, p. 421–431, doi:10.1016/j.epsl.2007.07.045.

Styron, R.H., Taylor, M.H., Sundell, K.E., Stockli, D.F., Oalmann, J.A.G., Möller, A., McCallister, A.T., Liu, D., and Ding, L., 2013, Miocene initiation and acceleration of extension in the South Lunggar rift, western Tibet: Evolution of an active detachment system from structural mapping and (U-Th)/He thermochronology: Tectonics, v. 32, no. 4, p. 880–907, doi:10.1002/tect.20053.

Suppe, J., and Medwedeff, D.A., 1990, Geometry and kinematics of fault-propagation folding, *in* Jordan, P., Noack, T., Schmid, S., and Bernoulli, D., eds., The Hans Laubscher Volume, Volume 83: Basel, Birkhaeuser Verlag, p. 409–454.

Villamor, P., and Berryman, K., 2001, A late Quaternary extension rate in the Taupo Volcanic Zone, New Zealand, derived from fault slip data: New Zealand Journal of Geology and Geophysics, v. 44, no. 2, p. 243–269, doi:10.1080/00288306.2001.9514937.

Walker, R., and Jackson, J., 2004, Active tectonics and late Cenozoic strain distribution in central and eastern Iran: Tectonics, v. 23, doi:10.1029/2003TC001529.

Walsh, J.J., Nicol, A., and Childs, C., 2002, An alternative model for the growth of faults: Journal of Structural Geology, v. 24, no. 11, p. 1669–1675, doi:10.1016/S0191-8141(01)00165-1.

Watts, A.B., and Burov, E.B., 2003, Lithospheric strength and its relationship to the elastic and seismogenic layer thickness: Earth and Planetary Science Letters, v. 213, no. 1–2, p. 113–131, doi:10.1016/S0012-821X(03)00289-9.

Wells, D.L., and Coppersmith, K.J., 1994, New empirical relationships among magnitude, rupture length, rupture width, rupture area, and surface displacement: Bulletin of the Seismological Society of America, v. 84, p. 974–1002.

Wesnousky, S.G., Kumar, S., Mohindra, R., and Thakur, V.C., 1999, Uplift and convergence along the Himalayan Frontal Thrust of India: Tectonics, v. 18, no. 6, p. 967–976, doi:10.1029/1999TC900026.

Whipple, K.X., 2009, The influence of climate on the tectonic evolution of mountain belts: Nature Geoscience, v. 2, p. 97–104, doi:10.1038/ngeo413.

Wickham, J., 1995, Fault displacement-gradient folds and the structure at Lost Hills, California (U.S.A.): Journal of Structural Geology, v. 17, no. 9, p. 1293–1302, doi:10.1016/0191-8141(95)00029-D.

Willenbring, J., and von Blanckenburg, F., 2010, Long-term stability of global erosion rates and weathering during late-Cenozoic cooling: Nature, v. 465, no. 7295, p. 211–214, doi:10.1038/nature09044.

Willett, S., Beaumont, C., and Fullsack, P., 1993, Mechanical model for the tectonics of doubly vergent compressional orogens: Geology, v. 21, no. 4, p. 371–374, doi:10.1130/0091-7613(1993)021<0371:MMFTTO>2.3.CO;2.

Willett, S.D., and Brandon, M.T., 2002, On steady states in mountain belts: Geology, v. 30, no. 2, p. 175–178, doi:10.1130/0091-7613(2002)030<0175:OSSIMB>2.0.CO;2.

Willett, S.D., Fisher, D., Fuller, C., En-Chao, Y., and Lu, C.Y., 2003, Erosion rates and orogenic-wedge kinematics in Taiwan inferred from fission-track thermochronometry: Geology, v. 31, no. 11, p. 945–948, doi:10.1130/G19702.1.

Wilson, C.J.N., Houghton, B.F., McWilliams, M.O., Lanphere, M.A., Weaver, S.D., and Briggs, R.M., 1995, Volcanic and structural evolution of Taupo Volcanic Zone, New Zealand: A review: Journal of Volcanology and Geothermal Research, v. 68, no. 1–3, p. 1–28, doi:10.1016/0377-0273(95)00006-G.

Wobus, C., Whipple, K.X., Kirby, E., Snyder, N., Johnson, J., Spyropolou, K., Crosby, B., and Sheehan, D., 2006, Tectonics from topography: Procedures, promise, and pitfalls, *in* Willett, S.D., Hovius, N., Brandon, M.T., and Fisher, D.M., eds., Tectonics, Climate, and Landscape Evolution: Geological Society of America Special Paper 398, p. 55–74, doi: 10.1130/2006.2398(04).

Zeitler, P.K., Koons, P.O., Bishop, M.P., Chamberlain, C.P., Craw, D., Edwards, M.A., Hamidullah, S., Jan, M.Q., Khan, M.A., Khattak, M.U.K., Kidd, W.S.F., Mackie, R.L., Meltzer, A.S., Park, S.K., Pecher, A., Poage, M.A., Sarker, G., Schneider, D.A., Seeber, L., and Shroder, J.F., 2001, Crustal reworking at Nanga Parbat, Pakistan: Metamorphic consequences of thermal-mechanical coupling facilitated by erosion: Tectonics, v. 20, no. 5, p. 712–728, doi:10.1029/2000TC001243.

Zhang, L., 2005, Engineering Properties of Rocks, First Edition: Amsterdam, London, Elsevier.